Technical Report 1237

Analysis and Implementation of Robust Grasping Behaviors

Camille Z. Chammas

MIT Artificial Intelligence Laboratory

Analysis and Implementation of Robust Grasping Behaviors

by

Camille Z. Chammas

S.B (1988) Mechanical and Materials Engineering
Vanderbilt University

**Submitted to the Department of
Mechanical Engineering
in Partial Fulfillment of the Requirements
for the Degree of Master of Science**

in Mechanical Engineering

at the

Massachusetts Institute of Technology

May, 1990

©Massachusetts Institute of Technology 1990
All rights reserved

Analysis and Implementation of Robust Grasping Behaviors

by

Camille Z. Chammas

Submitted to the Department of Mechanical Engineering on May 11, 1990 in partial fulfillment of the requirements for the Degree of Master of Science in Mechanical Engineering

Abstract: This thesis addresses the problem of developing automatic grasping capabilities for robotic hands. Using a 2-jointed and a 4-jointed model of the hand, we establish the geometric conditions necessary for achieving form closure grasps of cylindrical objects. We then define and show how to construct the grasping pre-image for quasi-static (friction dominated) and zero-G (inertia dominated) motions for sensorless and sensor-driven grasps with and without arm motions. The grasping pre-image is the area within which the object to be grasped must lie in order to be grasped successfully. The size and shape of this area depends upon the hand and object geometry and can be increased by employing sensor triggered actions (behaviors). While the approach does not rely on detailed modeling, it is computationally inexpensive, reliable, and easy to implement. Example behaviors were successfully implemented on the Salisbury hand and on a planar 2-fingered, 4 degree-of-freedom hand.

Thesis Supervisor:

J. Kenneth Salisbury, Jr.
Research Scientist
MIT AI Laboratory

Acknowledgments

This thesis describes research conducted at the Artificial Intelligence Laboratory at the Massachusetts Institute of Technology. Support for the laboratory's artificial intelligence research is provided in part by NASA Grant NAG-9-319, and in part by the Advanced Research Projects Agency of the Department of Defense under Office of Naval Research contract N00014-85-K-0124.

This work would not have been possible without the commitment and support from my advisor, Ken Salisbury. I would like to thank him for his unique insight and guidance. He has always been encouraging and enthusiastic and it has been a genuine pleasure working with him.

I would especially like to thank Sundar Narasimhan for his prominent ideas and insight benefiting my research. I cannot count the number of times or ways he has helped me. Most of all he has been a great source of inspiration, a great friend, and a great person to be around. Captain thank you very much.

Brian Eberman, and Dave Brock, were always there to answer enumerable questions. Mike Levin, and Tom Moyer, were always ready to machine mechanical parts for the hand. Thanks especially to Thomas Massie who stayed up late building the palm sensor and getting it to work. Thanks guys.

I would also like to thank David Siegal for all his help, Pete Maloney for helping out with AutoCad, and Emile for being a loving brother and helping to debug this thesis. I would like to thank Peng Wu, my office mate, for his company, for answering all my telephone calls, and for sharing his patched bean bag. Thanks to Michael Kashket for helping phrase some of the difficult concepts in this thesis.

Thanks to all my friends at MIT who have made my stay here valuable, and those at the Artificial Intelligence Laboratory for making it the unique place it is.

Special thanks goes to the GANG: Monique, Mariano, Pete, Jeannie, Doug, Mama Chanelle, Jeannie and Christine. Guys let's play those tunes again.

And last but not least, I would like to thank my parents for their support and love. They offered words of wisdom and confidence all along.

Contents

1 Introduction 9

1.1 Introduction 9

1.2 Overview 9

1.3 Outline 11

2 Necessary Conditions for Grasping: 2-Jointed Hand 13

2.1 Model Assumptions 13

2.2 Geometric Constraints 15

2.2.1 Algorithm 15

2.2.2 Example 21

2.2.3 Discussion 23

2.3 Extension to Convex Polygons 24

3 Quasi Static Grasping Region: 2-Jointed Hand 27

3.1 Definitions 27

3.2 Theoretical Analysis and Assumptions 29

3.3 Sensorless Behaviors 33

3.3.1 Grasping Region 33

3.3.2 Example 37

3.3.3 Arm Motion Behaviors 37

3.4 Sensory Behaviors 40

3.4.1 Grasping Region 40

3.4.2 Arm Motion Behaviors 40
3.4.3 Discussion 44

4 Zero-G Grasping; 2-Jointed Hand **46**
4.1 Theoretical Analysis 46
4.1.1 Equations of Motion During Contact 46
4.1.2 Equations of Motion During Impact 49
4.2 Sensorless Behaviors 51
4.2.1 Grasping Region 51
4.2.2 Example 55
4.3 Sensory Behaviors 55
4.3.1 Matching Velocities 56
4.3.2 Reducing Impact forces 56

5 Extension to a 4-Jointed Hand **59**
5.1 Necessary Conditions for Grasping 59
5.1.1 Necessary Conditions For Grasping 59
5.1.2 On hand designs 66
5.2 Quasi Static Grasping Region 69
5.2.1 Theoretical Analysis and Assumptions 69
5.2.2 Sensorless Behaviors 73
5.2.3 Sensory 74
5.3 Zero-G Grasping 75
5.3.1 Sensorless 75
5.3.2 Sensory 76

6 2-D Implementation **78**
6.1 Hardware Set-Up 78
6.2 2-Jointed Hand 80

6.2.1 Quasi Static Grasping 81
6.2.2 Zero-G Grasping 82
6.3 4-Jointed Hand 83

7 Implementation on the Salisbury Hand **85**
7.1 Experimental Set-Up 85
7.1.1 Hardware 85
7.1.2 Software 87
7.2 Extensions to 3-D Grasps 88
7.3 Implementations 90
7.3.1 Grasping a Cylinder on Constrained Surface 90
7.3.2 Grasping a Free Floating Cylinder 91

8 Conclusion **92**
8.1 Review 92
8.2 Future Work 93

List of Figures

2.1 2-D Model of Hand and Object 14
2.2 Force Closure Grasp 17
2.3 Form Closure Grasp with Structural Constraint 18
2.4 Form Closure Grasps Relying on Friction 18
2.5 Illustration for Minimum and Maximum Graspable Cylinder Radius (for Structural Form Closure, Rs, and Frictional Force Closure, R) . . 22
2.6 Finger Tip Geometry 23
2.7 Graspability of a Convex Polygon Independent of its Orientation . . . 25
2.8 Graspability of a Convex Polygon Dependent on its Orientation . . . 26

3.1 Notation 30
3.2 Pre-Image for a Sensorless Hand without a Constraining Surface . . . 34
3.3 Coordinate System 36
3.4 Pre-Image for Move and Grab 39
3.5 Hand and Sensors 43
3.6 First Contact Region 44
3.7 Comparison of Sensorless and Sensory Pre-Images 45

4.1 Zero-G Coordinate System 47
4.2 Impact Diagram 50
4.3 Cylinder's Motion In Between Impacts 53
4.4 Zero-G Grasping Pre-Image for a Sensorless Hand 55

5.1 4-Jointed Hand 60

5.2 Four Possible Structural Form Closure Grasps 62
5.3 Maximum Dimensionless Radius R^* for Case 1 63
5.4 Maximum Dimensionless Radius R^* for Case 2 64
5.5 Maximum Dimensionless Radius R^* for Case 3 65
5.6 Maximum Dimensionless Radius R^* for Case 4 66
5.7 Maximum Dimensionless Radius R^* of All Four Cases 67
5.8 Optimal Geometries for Hands 69
5.9 Notation 70
5.10 Behavior Conditioned for an Object Approaching Normal to the Wrist Surface 77

6.1 2-D Experimental Set-Up 78
6.2 Experimental Quasi-Static Whole Grasping Region for a Sensorless 2-Jointed Hand 81
6.3 Experimental Zero-G Grasping Pre-Image for a Sensorless 2-Jointed Hand 82

7.1 3-D Experimental Set-Up 86
7.2 3-D Zero-G Pre-Image for a Sensorless Hand 89

Chapter 1

Introduction

1.1 Introduction

When grabbing pens, cups or other similar objects, humans frequently reach out and grab without consciously planning the trajectories of their arms, hands, or fingers. Such simple manipulation tasks rely upon unconscious behaviors triggered by sensory information. For example, infants close their fingers when pressure is applied on their palms. Force applied on the top of the hand will cause the hand and arm to withdraw briefly and return to grasp near the original point. [1] These basic behaviors seem sufficient to perform a useful range of primitive grasping motions.

This thesis suggests an approach to solve simple grasping problems. The focus is on grasping of imprecisely defined objects with an imprecisely defined hand. The emphasis is on acquisition of the object more than achieving a precise final pose of the grasped object.

1.2 Overview

There have been two principal approaches to grasping. The first relies on accurate geometric models of the world. The second relies upon primitive behaviors that accomplish somewhat intelligent actions.

[Nguyen 86] has developed an algorithm to generate independent regions of finger contact for polyhedral objects that would result in a stable force-closure grasp.

[1] A wide range of stimuli (such a noise, acceleration or change of contact force) will trigger the Morrow reflex in infants (a clinging posture which helps protect infants from falling).

Building on Nguyen's work, [Pollard 89] has addressed the problem of planning the motion of a robot arm with a three-fingered hand so that it will accomplish a given grasping task.

On the other end of the spectrum, Brooks[86] built "insect" robots with layers of primitive behaviors that accomplish somewhat intelligent tasks. Dedieu, Degrange, and Sailly[89] built a simulator to test a set of grasping behaviors for a planar two fingered hand. Four sets of behaviors were layered in a subsumption-like architecture. Unfortunately, the set of chosen behaviors did not accomplish the desired task. Others have developed heuristic approaches to robot grasping manipulation. Stansfield[89] developed a knowledge-based approach for grasping unknown objects. A set of hand preshapes and a set of wrist orientations with a ballistic reach were used for grasping operations.

The physics underlying pushing operations has also been studied to accomplish useful tasks. [Mason 85] studied the mechanics of pushing operations and found a method for determining which way a pushed object will rotate. Erdmann and Mason[88] used sensorless manipulations to orient planar parts. A series of tray tilting operations were performed to orient a wrench without the use of sensors. Peshkin and Sanderson[88] developed techniques to study the motion of a sliding workpiece. These techniques were consequently used for planning open loop (sensorless) manipulation tasks. Trinkle[89] has developed algorithms to predict the instantaneous velocity of an object undergoing quasi-static manipulation.

This work examines the motion of cylinders when pushed by a rotating link. The physics behind this pushing operation is studied to develop behaviors that will use such strategies to grasp cylinders. Unlike Peshkin and Sanderson[88], and Trinkle[89], we are not interested in knowing the exact motion of the sliding workpiece. Assumptions about material properties, friction, and other physical phenomena are made to provide conservative answers that also simplify the analytical solution. Even though

this approach addresses a limited class of objects, it is computationally inexpensive, reliable, and easy to implement.

1.3 Outline

This thesis describes a new approach using reflexive behaviors that guarantee grasping. A reflexive behavior is defined to be a set of hand/arm motions triggered by sensory information.

We chose to focus on cylinders because many useful objects can be treated as cylinders for simple grasping. The resulting methods allow us to specify the necessary preconditions which must be satisfied in order to successfully grasp a cylinder even in the presence of known uncertainties.

In Chapter 2, a 2-jointed hand model is introduced. We model the fingers as lines and identify both grasps which can encircle the object (structural form closure grasps) and grasps which rely on friction to constrain the object. Necessary conditions are derived for grasping cylinders successfully. These conditions define the range of object sizes that can be acquired given a particular hand geometry. A simple method for extending this analysis to convex polygons is proposed.

In Chapter 3, sensorless and sensory behaviors are developed for grasping cylinders when their motion is dominated by friction. This would be equivalent to grasping a cylinder lying on a table. Then we look at how these behaviors modify the "grasping regions" (regions where the object should be located, relative to the hand prior to grasping, in order to guarantee acquisition).

Chapter 4 presents sensorless and sensory behaviors using the 2-jointed model for freely floating objects in space. A theoretical analysis of the dynamics between the hand and the cylinder is presented. The results of the analysis are used in conjunction with sensorless and sensory behaviors to derive grasping regions.

Chapter 5 extends the ideas developed in chapter 2, 3 and 4 to a 4-jointed hand

model. More complex behaviors made possible with this more complicated model are analyzed and compared with the 2-jointed hand. Some useful insights into hand design result from this analysis.

In Chapter 6, a planar 2-Fingered hand is used to test the validity of the grasping regions developed for the 2-jointed and 4-jointed hand. Upper limits on closing speeds are also determined experimentally.

Chapter 7 presents a 3-D implementation of several grasping behaviors using the *Salisbury* hand mounted on a *Puma* arm guided by a vision system. While the analyses used are essentially 2-D in nature, they can be applied to a number of true 3-D grasping situations. Two types of grasping modes (tip prehension and cylindric) are used for this implementation. A cylindric grasp is a mode which occurs when the hand approaches a cylinder (assumed to be of infinite length) normal to its axis of rotation, while a tip prehension mode occurs when the hand approaches the cylinder (or a disk) from its end along its axis of symmetry and uses three fingertips to constrain the disk. These grasping modes combined with the sensory behaviors developed in earlier chapters are implemented to grasp "free floating" cylinders.

Chapter 2

Necessary Conditions for Grasping: 2-Jointed Hand

A 2-d model of a hand with two fingers (one link per finger) is developed and studied in the following three chapters. This chapter establishes necessary conditions for grasping a circle (i.e. the projection of a cylinder along its rotational axis of symmetry onto a plane) given the dimensions of the hand and the coefficient of friction between the hand and object to be grasped. In subsequent chapters, we study behaviors that establish sufficient conditions for grasping cylinders.

In choosing how to grasp an object it must first be decided if it is graspable at all. The following sections establish necessary geometric conditions which must be satisfied in order to grasp a cylinder with a simple 2-jointed hand.

Before the geometric constraints are established, the 2-jointed hand model is discussed with respect to all the assumptions. Even though the geometric constraints are derived for cylinders, an extension to convex polygons is proposed.

2.1 Model Assumptions

The 2-D model and all pertinent information are shown in Figure 2.1.

The following assumptions are made during our analysis:

1. The fingers are open before the grasping motion begins.

2. The two fingers close at the same speed, hence the final grasp is symmetric.

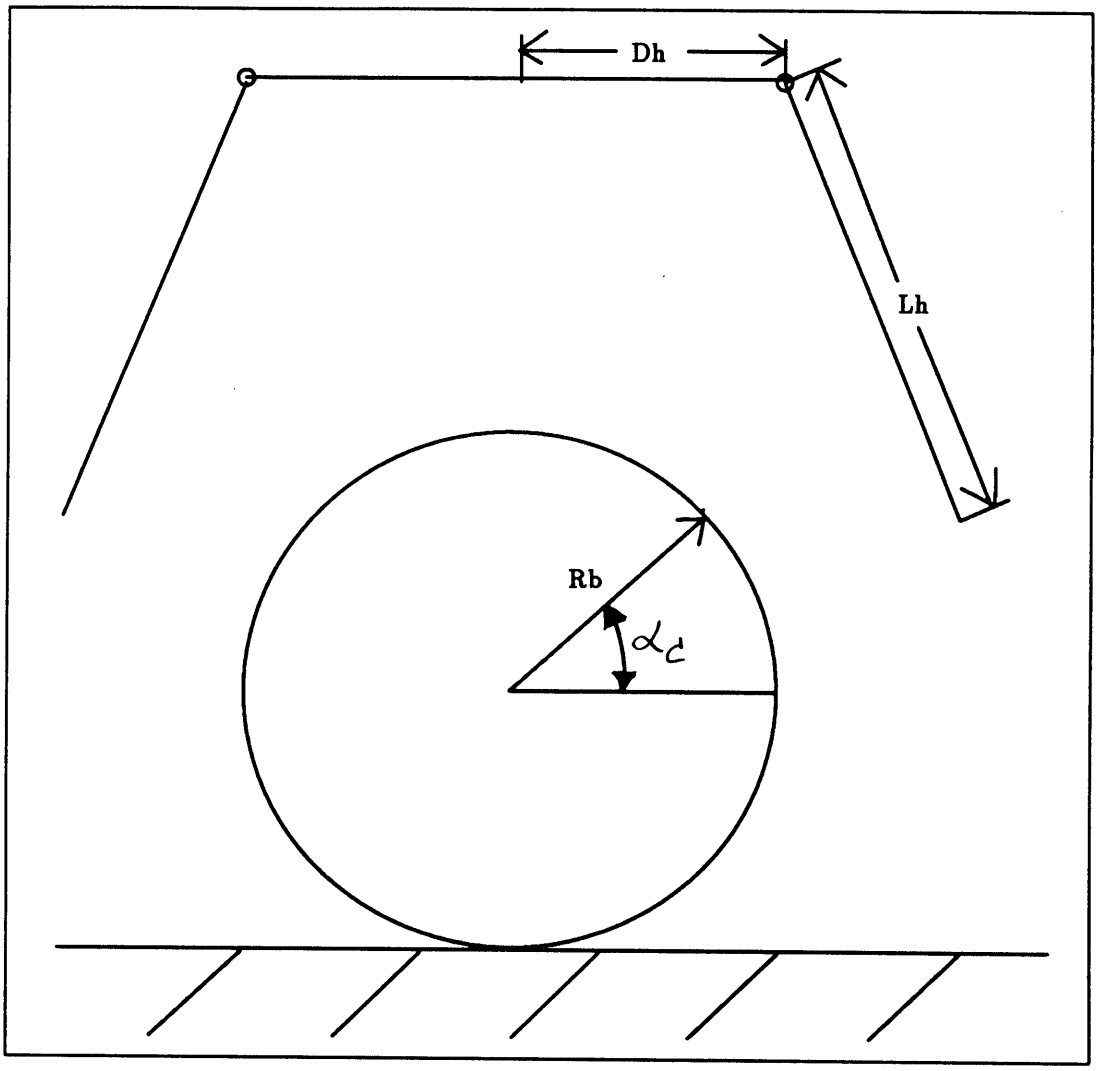

Figure 2.1: 2-D Model of Hand and Object

3. The fingers are allowed to intersect, which allows form closure grasps. (This is physically possible, if the fingers move in different, parallel planes).

4. The object is light enough so that the fingers can exert enough force to lift it. The mass of the object can then be ignored.

5. Movement is quasi-static so dynamic effects are negligible.

6. The wrist orientation is fixed.

7. The hand base (wrist) is compliant for translations with respect to its environment.

The implications and validity of these assumptions will be discussed later.

2.2 Geometric Constraints

The following analysis establishes conditions that must be satisfied in order to allow the grasping of cylinders. The range of cylinder diameters which may be grasped is determined for a given hand. Alternately, the results may be used to tell us how large a hand must be to grasp a given set of cylinders.

2.2.1 Algorithm

The following definitions are used throughout this chapter:

1. *Force Closure Grasp*: Is a grasp that is maintained stable by an external force. This type of grasp will not be considered in this analysis because of stability and manipulation reasons, but an example is provided in Figure 2.2.

2. *Form Closure Grasp*: Is a grasp that can resist arbitrary external disturbances. Two cases of form closure grasps will be considered. The first, as illustrated in Figure 2.4, is a form closure grasp relying on the friction between the hand and the object. The second, as illustrated in Figure 2.3, is a form closure grasp with structural constraint. In both cases the grasp may be maintained against external forces by squeezing more tightly.

3. R_{min}: The radius of the smallest cylinder that can be grasped while relying on the friction between the finger and the cylinder.

4. R_{max}: The radius of the largest cylinder that can be grasped while relying on the friction between the finger and the cylinder.

5. R_{smin}: The radius of the smallest cylinder that can be grasped using form closure with structural constraint.

6. R_{smax}: The radius of the largest cylinder that can be grasped using form closure with structural constraint.

7. L_h: The finger length.

8. D_h: The half wrist length.

9. α_c: The friction cone angle = $\arctan(\mu)$

10. α_a: When the friction cone angle, α_c, exceeds α_a, the minimum graspable radius is limited by geometry and not friction.

11. α_{cc}: The friction angle that sets a limit to grasping. If the friction cone angle, α_c, is smaller than α_{cc}, grasping is impossible.

12. β: D_h/L_h, the ratio of the half wrist length to the finger length.

13. μ: The coefficient of friction.

The following algorithm determines the size of cylinders graspable with a given hand geometry. The fingers and wrist are treated as lines and the cylinder as a circle. The problem is reduced to a geometric problem. Conditions are derived to prevent the lines from intersecting the circle which is equivalent to preventing the hand from crushing the cylinder. Conditions for form (structural and frictional) closure are also prescribed. Form closure grasps relying on friction are less secure because they rely on friction to maintain the grasp, but they are geometrically less restrictive and enable the grasping of a broader range of objects.

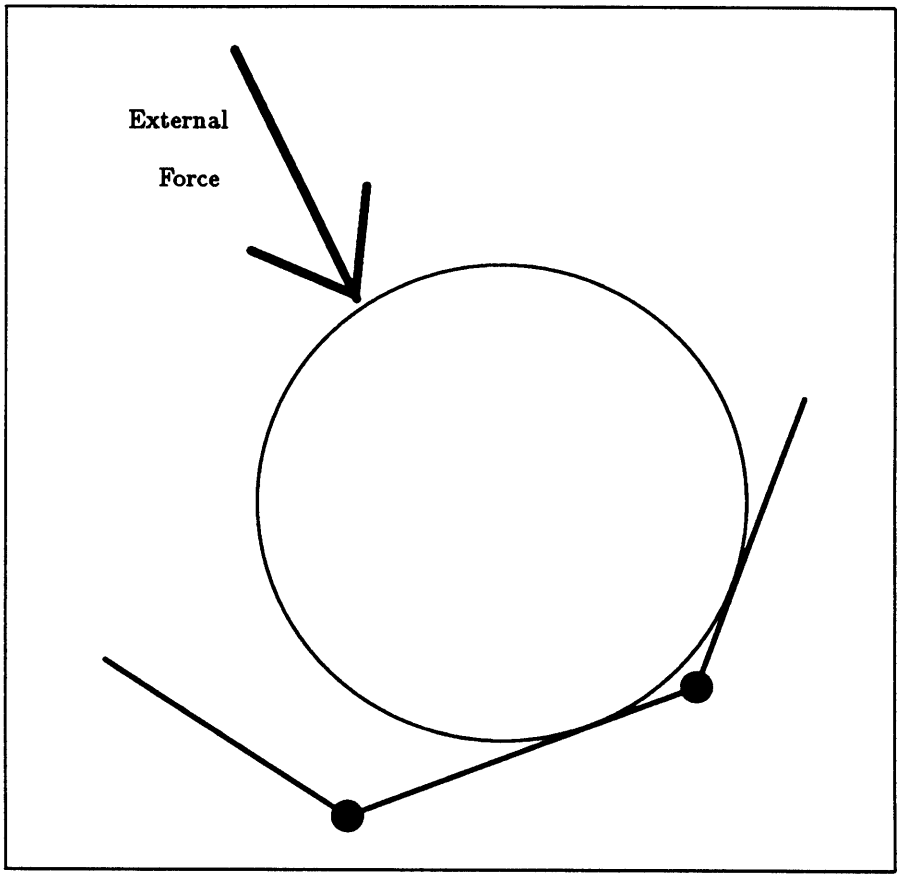

Figure 2.2: Force Closure Grasp

The equations below give the limits of graspable object size for both types (structural and frictional) of form closure grasp on a cylinder. $\beta = \frac{D_h}{L_h}$, a dimensionless quantity, is defined to simplify the solution. If $\beta \leq 1$ the solution is very simple, as outlined in the following algorithm. If $\beta > 1$ a quadratic equation needs to be solved. δ is defined as the square root term that arises from the solution of this quadratic equation. α_{cc} is the angle that sets δ to zero, and this represents the condition for grasping. It can be proved, that if the roots are real they are always positive; which guarantees the existence of a positive radius. α_a is the condition for two circles to intersect at one point while maintaining the condition for intersection. The circle

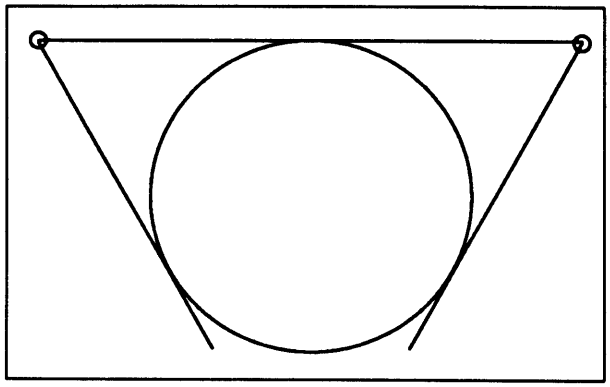

Figure 2.3: Form Closure Grasp with Structural Constraint

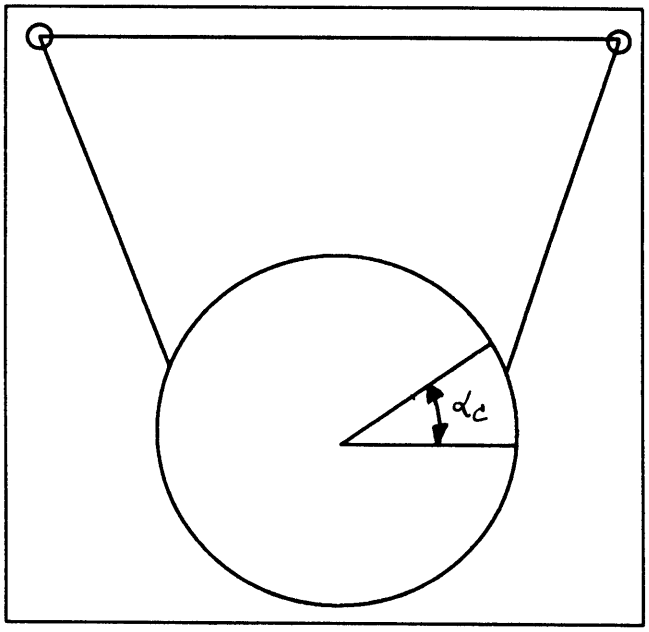

Figure 2.4: Form Closure Grasps Relying on Friction

that satisfies the previous equations is the smallest circle that can be grasped by the hand independent of the coefficient of friction. The expression for α_a was simplified using half-angle trigonometric relations.

1. Define β as:

$$\beta = \frac{D_h}{L_h}$$

2. Define α_c as:

$$\alpha_c = \arctan(\mu)$$

3. Define α_{cc} as:

$$\alpha_{cc} = \arcsin\left(1 - \frac{2}{\beta^2}\right)$$

Case 1: $\beta \leq 1$

$$\begin{aligned} \frac{R_{min}}{L_h} &= 0 \\ \frac{R_{smin}}{L_h} &= 0 \\ \frac{R_{max}}{L_h} &= \frac{(\beta + \sin\alpha_c)}{\cos\alpha_c} \\ \frac{R_{smax}}{L_h} &= \beta \end{aligned} \tag{2.1}$$

Case 2: $1 < \beta \leq \sqrt{2}$

$$\begin{aligned} \frac{R_{smin}}{L_h} &= \frac{\beta - \sqrt{2-\beta^2}}{2} \\ \frac{R_{smax}}{L_h} &= \frac{\beta + \sqrt{2-\beta^2}}{2} \end{aligned} \tag{2.2}$$

To compute $\frac{R_{min}}{L_h} and \frac{R_{max}}{L_h}$ follow the procedure for $\sqrt{2} < \beta$.

Case 3: $\sqrt{2} < \beta$

1. Define α_a as:

$$\alpha_a = 2 \arctan\left(\frac{\beta - 1}{\beta + 1}\right)$$

2. If $0 < \alpha_c < \alpha_a$

   (a) if $\alpha_c < \alpha_{cc}$ then there is NO POSSIBLE grasp.

   (b) if $\alpha_c = \alpha_{cc}$ then:

$$R_{min} = R_{max} = \frac{\beta\sqrt{\beta^2 - 1}}{2}$$

   (c) if $\alpha_{cc} < \alpha_c$ then

$$\begin{aligned} \delta &= \sqrt{2(1 - \sin\alpha_c) - \beta^2(\sin\alpha_c - 1)^2} \\ \frac{R_{min}}{L_h} &= \frac{\beta\cos\alpha_c - \delta}{2(1 - \sin\alpha_c)} \\ \frac{R_{max}}{L_h} &= \frac{\beta\cos\alpha_c + \delta}{2(1 - \sin\alpha_c)} \end{aligned} \tag{2.3}$$

3. if $\alpha_a < \alpha_c$ then

$$\begin{aligned} \frac{R_{min}}{L_h} &= \frac{\beta^2 - 1}{2} \\ \frac{R_{max}}{L_h} &= \frac{\beta\cos\alpha_c + \delta}{2(1 - \sin\alpha_c)} \end{aligned} \tag{2.4}$$

2.2.2 Example

The following example illustrates the use of the above algorithm for a hand with the following dimensions:

1. Finger length: $L_h = 1.0$
2. Wrist half length: $D_h = 1.2$

The above proportions were chosen to give more insight to the solution by showing how the type of form closure can be achieved for different size cylinders.

First, it is found that $\beta = 1.2$. Equations 2.2 are used to compute the minimum and maximum radius that can be grasped using structural form closure because $1 < \beta \leq \sqrt{2}$, and equations 2.3 to compute the maximum and minimum radius that can be grasped using a friction coefficient of 0.7. This example yields the following results:

$$\begin{aligned} \beta &= 1.2 \\ \alpha_c &= 35^\circ \\ \alpha_{cc} &= -22.9^\circ \\ \alpha_a &= 10.4^\circ \\ R_{smin} &= 0.226 \\ R_{smax} &= 0.974 \\ \delta &= 0.769 \\ R_{min} &= 0.220 \\ R_{max} &= 2.054 \end{aligned} \tag{2.5}$$

Figure 2.5 illustrates these results.

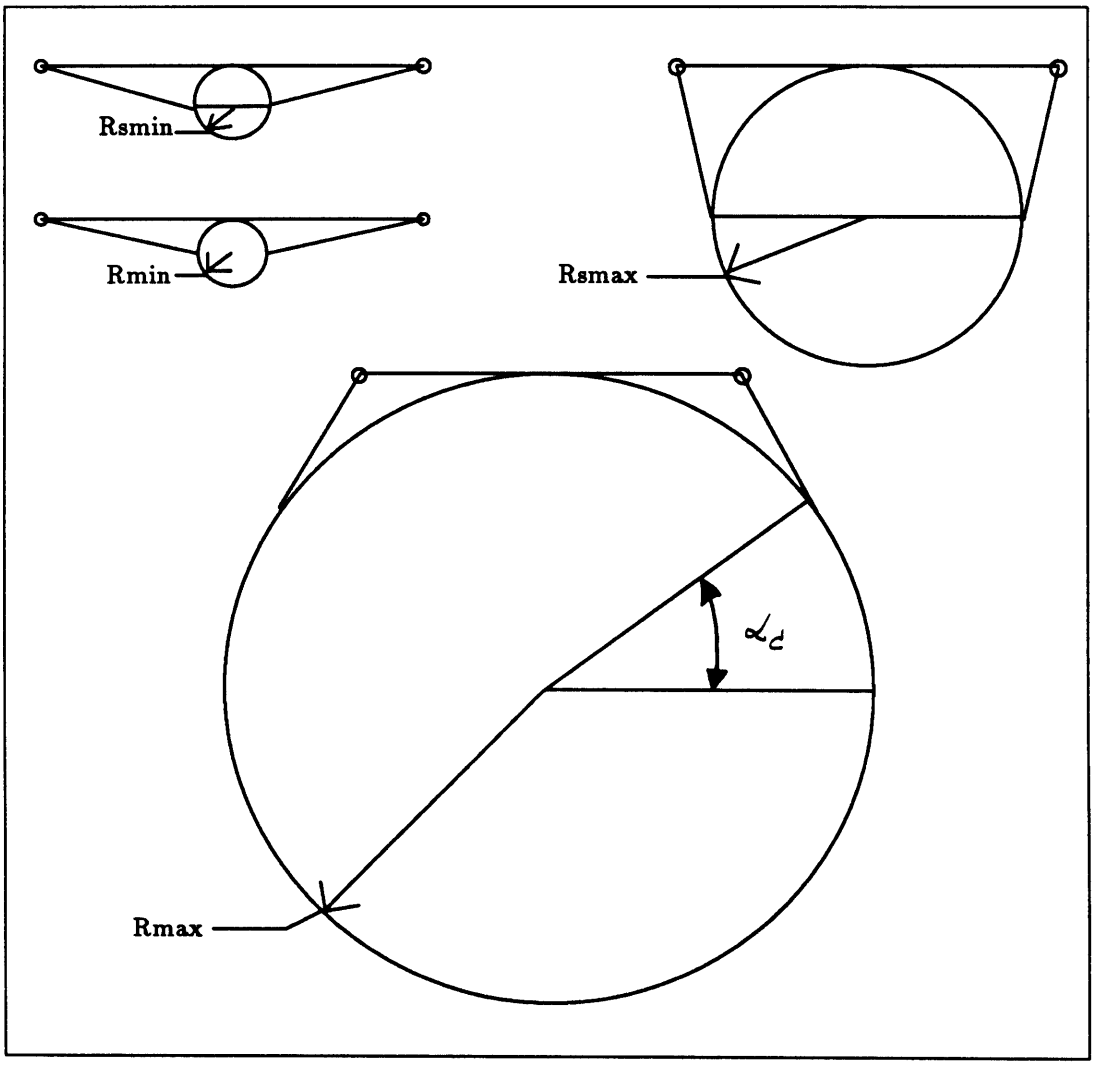

Figure 2.5: Illustration for Minimum and Maximum Graspable Cylinder Radius (for Structural Form Closure, Rs, and Frictional Force Closure, R)

2.2.3 Discussion

Whenever the radius of the cylinder is set to zero, it is implied that the hand can grasp a circle of a very small radius. In fact, the limiting size for the radius is the finger tip and not the hand geometry. In an actual design such as the Salisbury hand, the finger tips are spherical, so the limiting factor is the finger tip diameter. An illustration of this point is given in Figure 2.6.

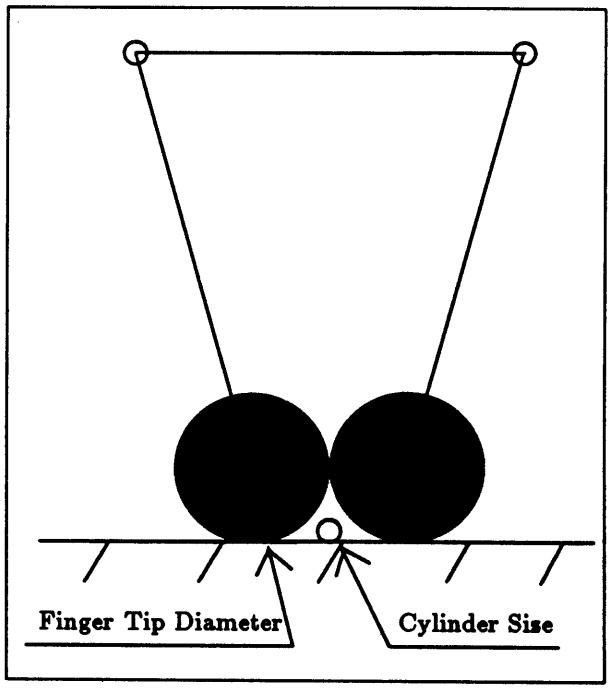

Figure 2.6: Finger Tip Geometry

Even though this is a 2-D analysis, the 2-D results can be applied to the 3-D case. In fact, if the hand and the circle are projected into the paper, the problem becomes of that of a 3-D hand grasping a cylinder. A 3-D analysis would provide more insight to the problem only if the objects being manipulated were small relative to the hand. The 2-D analysis is sufficient to handle the other cases.

Another useful result from this analysis is the relationship between the friction

coefficient and the maximum radius. The maximum graspable cylinder radius increases drastically with increases in the friction coefficient. The maximum radius increases as $\frac{1}{\cos \alpha_c}$. To maximize the radius it is very important to choose a large friction coefficient.

From a design standpoint, the following question needs to be addressed: What hand designs are capable of grasping a given range of cylinders? Solving for β in the above equations using simple algebra would answer this question. Equations (2.2) through (2.4) have been derived so as to simplify this task.

2.3 Extension to Convex Polygons

The above results can be extended to set conditions for grasping *convex polygons*. The following steps are suggested:

1. Use the above algorithm to find the lower and upper limit for grasping circles given a hand geometry.

2. Any convex polygon which cannot be inscribed by the above minimum circle, will be considered too small for grasping.

3. Any convex polygon which cannot be circumscribed by the largest circle, will be considered too large for grasping.

This is of course a conservative method but it guarantees graspability from any angle of approach. This is actually an important result because the hand can approach the object from any given angle and grasp it. Figure 2.7 shows an example of a convex polygon that meets the above criteria. Figure 2.8 demonstrates how a convex polygon which does not meet the third criteria but can still be grasped for a particular hand orientation. While this is a heuristic extension of the results for cylinders, it provides a quick way to check for graspability of irregularly shaped objects.

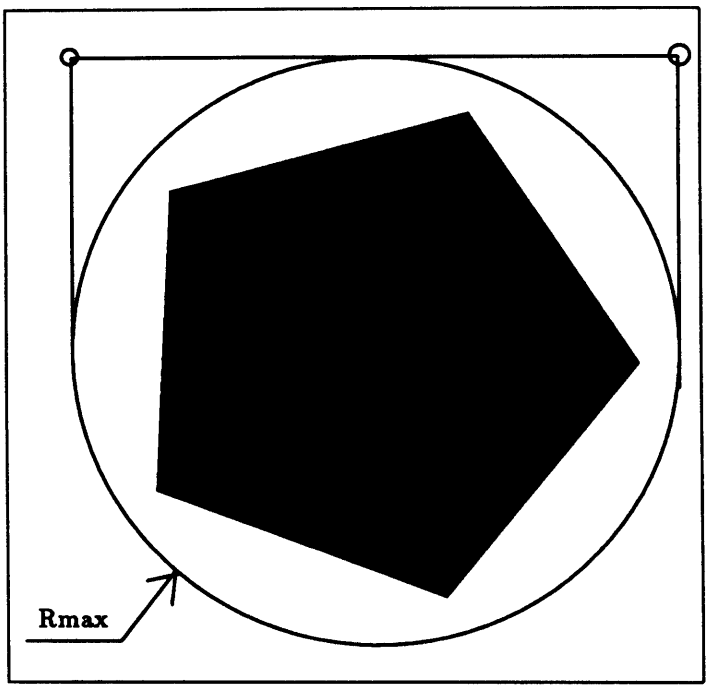

Figure 2.7: Graspability of a Convex Polygon Independent of its Orientation

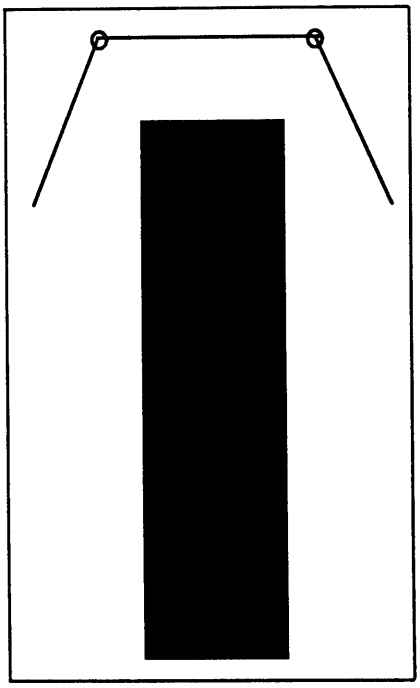

Figure 2.8: Graspability of a Convex Polygon Dependent on its Orientation

Chapter 3

Quasi Static Grasping Region: 2-Jointed Hand

This chapter looks at pushing operations on cylinders sliding on a horizontal surface which result in successful grasps. All motions of the cylinder are assumed to be *quasi static* and hence friction dominated. First, a theoretical analysis is presented to determine the motion of a cylinder being pushed by a rotating link. Sensorless and sensory behaviors, that can guarantee successful grasping, are developed based upon the equations of motion of the cylinder. These behaviors lead to grasping regions, areas within which the cylinder should be placed in order to guarantee grasping.

3.1 Definitions

The following terms need to be defined before proceeding in the analysis:

1. *Whole Grasping Region*: The region within which the entire cylinder must be located in order to guarantee grasping.

2. *Center Grasping Region*: The region within which the center of the cylinder must be located in order to guarantee grasping.

3. *Contact Grasping Region*: The region traced during the grasping motion by the contact point between the cylinder and the finger. The whole, center, and contact grasping regions contain equivalent information and may be derived from each other as shown in section 3.3.1.

4. *Pre-Image*: This term was first defined by Lozano-Perez, Mason, and Taylor [84]. In this thesis, we will use the term pre-image to denote the set of all

locations of the cylinder for which a given grasping motion will result in a successful grasp. All three grasping regions (whole, center, and contact) are referred to collectively as the pre-image.

5. *Sensorless Hand*: A hand without tactile sensors.

6. *Sensorless Behavior*: Arm and hand motion is planned *a priori* to the task and cannot be changed during execution of the motions.

7. *Sensory Behavior*: A set of pre-programmed arm and hand responses that are triggered upon sensor contact.

8. *Scooping*: A motion that will slide or roll the object towards the wrist by moving the arm in a given direction with the fingers open.

The three types of grasping regions have been defined for the following reasons. First, the notion of *Center Grasping Region* is useful for a high level planner. In fact, some planners use a C-Space approach to plan motions. The basic idea is to shrink the object to a point and extend the obstacles by the same proportion. Then, motion planning for a robot would be equivalent to finding a path for that point around the extended obstacles. For more details refer to Lozano-Perez[83]. The center grasping region has the same flavor in the sense that the center of the cylinder (ie. a point) has to be contained within that region. Second, the notion of *Whole Grasping Region* would be beneficial for a teleoperator. The teleoperator would place the hand around the cylinder such that it is fully contained within the grasping region. It is easier for humans to visualize the whole cylinder being inside a region than a point inside another region. Third, the notion of *Contact Grasping Region* has been defined because the grasping region is most simply described in terms of the contact point between the finger and the cylinder. Thus, the grasping regions are equivalent and may derived from each other. They are a function of hand design, cylinder radius, and friction coefficient.

The pre-image can be viewed from two perspectives:

1. Given the position of the hand, where should the object be located to guarantee grasping?

2. Given the position of the object, where can the hand be positioned to guarantee grasping?

This is actually two sides of the same coin. We choose to look at it from the first standpoint because it simplifies the analysis.

3.2 Theoretical Analysis and Assumptions [1]

Given a hand with two fingers (one link per finger), it is of interest to find the motion of a cylinder when it is pushed by a moving finger (link). It will be shown that if the moment exerted on the cylinder is equal to zero the rotation rates of the finger and the cylinder will be equal. First the velocity of a point on the cylinder due to the rotation of the finger and the cylinder will be derived. This velocity vector will be used to compute the direction of the frictional force component contributed by sliding of that point. We are assuming coulomb friction which implies that the magnitude of the frictional force is independent of the velocity. Finally, the total moment will be found by integrating the differential moments over the whole area of the cylinder. Equating this moment to zero permits us to solve for the cylinder's rotation rate and thus predict its motion when pushed.

The following terms are used throughout the derivation:

1. V1 : The velocity of a point on the cylinder due to the rotation of the finger.

2. V2 : The velocity of a point on the cylinder due to the rotation of the cylinder.

[1]This derivation was suggested by D.L.Brock

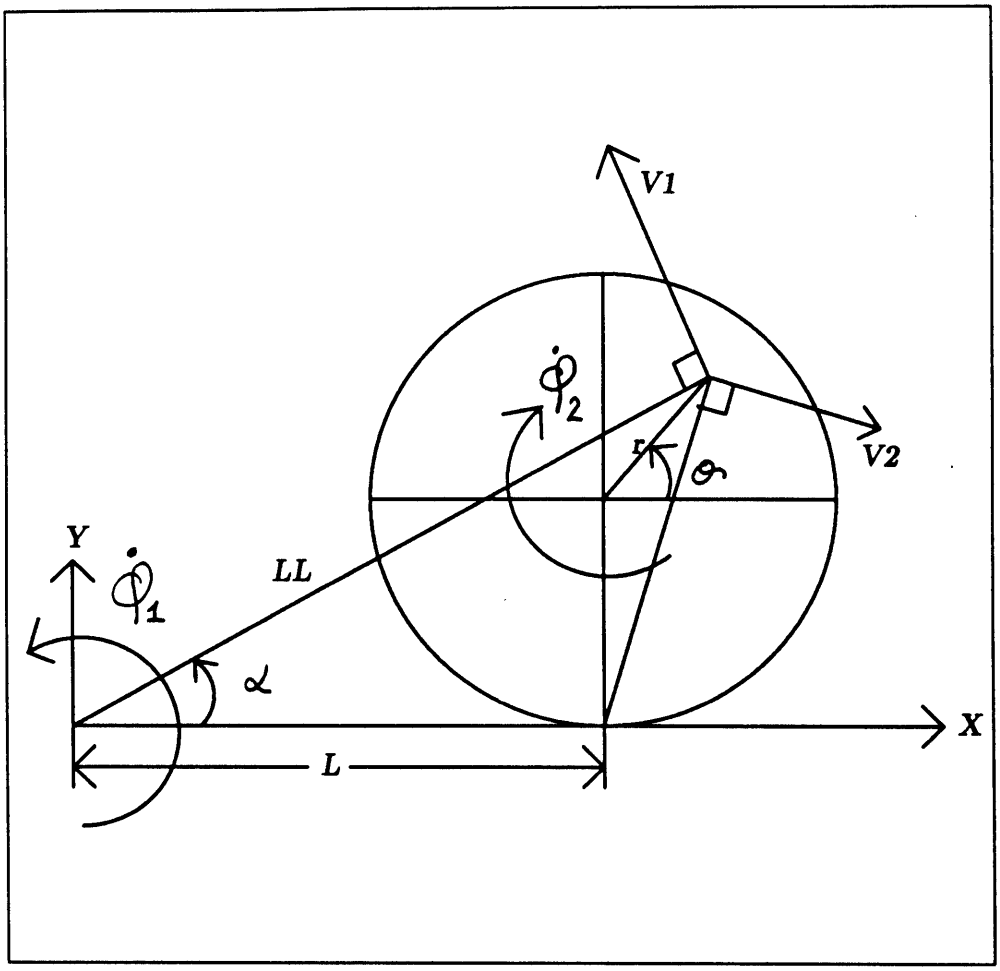

Figure 3.1: Notation

3. $\dot{\phi}_1$: The angular velocity of the link.

4. $\dot{\phi}_2$: The angular velocity of the cylinder.

5. *dm* : The differential moment.

6. *df* : The differential force.

7. M : The total moment on the cylinder.

8. $\mu(r,\theta)$: The friction coefficient.

9. $P(r,\theta)$: The pressure distribution function under the cylinder.

10. R : Radius of the cylinder

11. r : Distance from the center of the cylinder to a point on the cylinder.

12. LL : Distance between the reference frame and a point on the cylinder.

13. L : Distance between the reference frame and the contact point between the cylinder and the link.

14. m : Mass of the cylinder.

15. g : Gravity.

The other symbols are defined in Figure 3.1.

V1 is equal to:

$$V1 = \dot{\phi}_1 LL \begin{bmatrix} -\sin(\alpha) \\ \cos(\alpha) \end{bmatrix} \tag{3.1}$$

From geometry it can be shown that:

$$\begin{aligned} \sin(\alpha) &= \frac{R + r\sin(\theta)}{LL} \\ \cos(\alpha) &= \frac{L + r\cos(\theta)}{LL} \end{aligned} \tag{3.2}$$

Hence:

$$V1 = \dot{\phi}_1 \begin{bmatrix} -(R + r\sin(\theta)) \\ (L + r\cos(\theta)) \end{bmatrix} \tag{3.3}$$

Using the above method, V2 is equal to:

$$V2 = \dot{\phi}_2 \begin{bmatrix} R + r\sin(\theta) \\ -r\cos(\theta) \end{bmatrix} \tag{3.4}$$

The total velocity is found by adding the contribution of each rotation:

$$V = \begin{bmatrix} -(\dot{\phi}_1 - \dot{\phi}_2)(R + r\sin(\theta)) \\ (\dot{\phi}_1 - \dot{\phi}_2)r\cos(\theta) + L\dot{\phi}_1 \end{bmatrix} \tag{3.5}$$

If the two rotation rates are equal $\dot{\phi}_1 = \dot{\phi}_2$ then the velocity can be simplified to:

$$V = \begin{bmatrix} 0 \\ L\dot{\phi}_1 \end{bmatrix} \tag{3.6}$$

The frictional force at each point has a direction opposite to the velocity vector. The differential moment due to each differential force is equal to the cross product of the position vector and the frictional force vector:

$$dm = \begin{bmatrix} r\cos(\theta) \\ (R + r\sin(\theta)) \end{bmatrix} \times df \tag{3.7}$$

$$dm = \begin{bmatrix} r\cos(\theta) \\ (R + r\sin(\theta)) \end{bmatrix} \times \left[\mu(r,\theta)P(r,\theta)\frac{-V}{\|V\|}r\,dr\,d\theta\right] \tag{3.8}$$

The pressure distribution and the friction coefficient are assumed to be uniform under the cylinder(ie $\mu(r,\theta) = \mu$ and $P(r,\theta) = \frac{mg}{\pi R^2}$). After cross multiplying the pre-

vious equation and integrating over the whole area of the cylinder, the total moment on the cylinder was found to be:

$$M = -\mu \frac{mg}{\pi R^2} \int_0^R \int_0^{2\pi} r^2 \cos(\theta)\, d\theta\, dr \tag{3.9}$$

Which is equal to zero because the integral of $\cos(\theta)$ from zero to 2π is equal to zero. Thus it can be shown that if:

$$\frac{\dot{\phi}_1}{\dot{\phi}_2} = 1 \tag{3.10}$$

Then:

$$M = 0 \tag{3.11}$$

Therefore we can easily predict the motion of the cylinder as it is pushed by a finger and use this knowledge to derive sensorless and sensory behaviors.

3.3 Sensorless Behaviors

Hand arm motions without any touch feedback are considered in this section.

3.3.1 Grasping Region

It has been shown that the ratio of the angular rotation of the finger to that of the cylinder is equal to one when the cylinder is sliding on a surface with uniform pressure distribution. This implies that the cylinder rolls on the finger and maintains orientation during the grasping motion. This motion can now be used to build a pre-image that will guarantee grasping by finding all sets of the cylinder's initial positions that will end up in a stable grasp.

The following algorithm permits us to compute the pre-image of a sensorless hand:

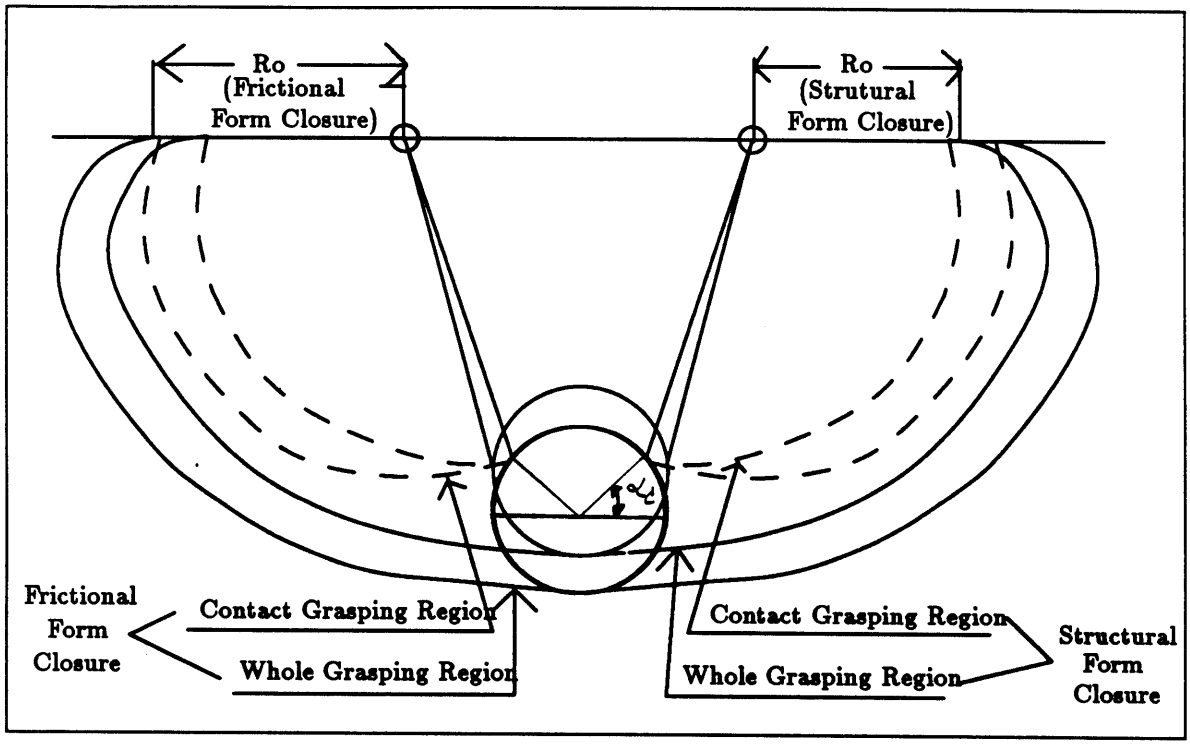

Figure 3.2: Pre-Image for a Sensorless Hand without a Constraining Surface

1. Compute θ from:

$$\theta = \arccos\left(\frac{D_h - R_b \cos\alpha_c}{L_h}\right)$$

2. Compute α_h from:

$$\alpha_h = \pi - \theta$$

3. Compute θ_i from:

$$\theta_i = \frac{L_h}{R_b} + \alpha_c$$

4. If $\theta_i + \theta > \pi$ then:

$$\begin{aligned} R_o &= (\theta_i + \theta - \pi) R_b \\ \theta_o &= 0 \end{aligned} \tag{3.12}$$

else

$$\begin{aligned} R_o &= 0 \\ \theta_o &= \pi - (\theta_i + \theta) \end{aligned} \tag{3.13}$$

5. A coordinate system is defined as shown in figure 3.3. The grasping region is obtained by plotting the points from the following equation:

$$R = R_o + R_b\theta$$

varying θ

$0 \leq \theta \leq (\alpha_k - \alpha_c)$

θ_o is the initial finger joint position as defined by the coordinate system, and R_o is the contact point between the circle and the finger at joint position θ_o. R is the contact point between the hand and the cylinder. The above equations yield the contact grasping region. To obtain the whole or center grasping region a shift operation would suffice. Instead of plotting the curve defined by R and θ; the whole grasping region is obtained by plotting the curve defined by R_w and θ_w defined by:

$$R_w = \sqrt{(R_o + R_b + R_b\theta)^2 + R_b^2}$$

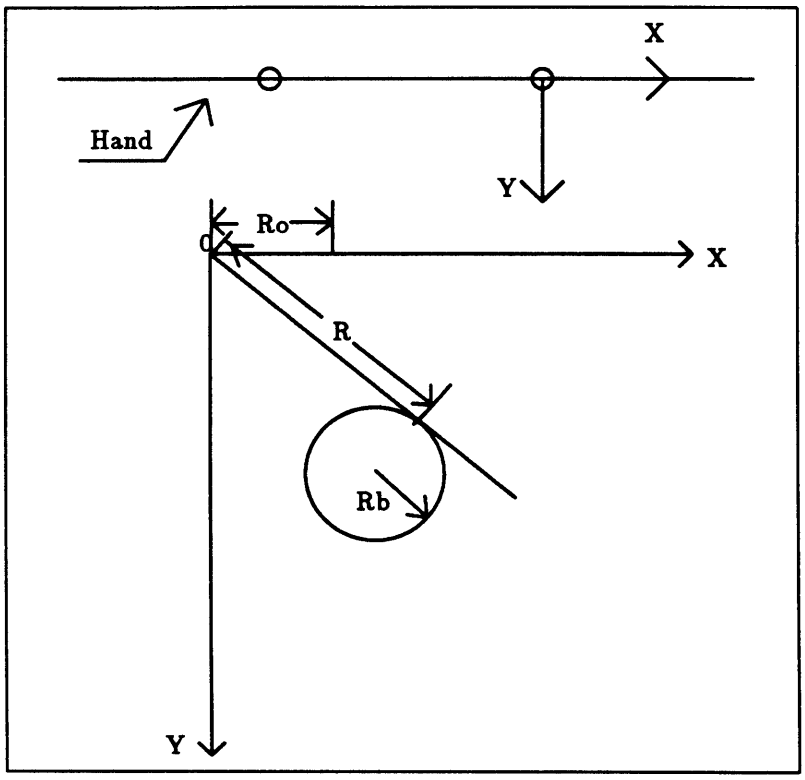

Figure 3.3: Coordinate System

$$\theta_w = \arctan\left(\frac{R_b}{R_o + R_b + R_b\theta}\right)$$

Similarly, the contact grasping region is obtained by plotting the curve defined by R_c and θ_c defined by:

$$R_c = \sqrt{(R_o + R_b\theta)^2 + R_b^2}$$

$$\theta_c = \arctan\left(\frac{R_b}{R_o + R_b\theta}\right)$$

As it has been shown, the equations for the grasping regions can be derived from one another. It is sufficient to specify one curve in order to derive the other two.

3.3.2 Example

The whole grasping image for this behavior is shown in Figure 3.2 using the following dimensions:

$$L_h = 2.0 \ ; \ D_h = 1.0$$

$$R_b = 0.5 \ ; \ \alpha_c = 35^\circ$$

The two regions shown in Figure 3.2 are the pre-images for structural and frictional form closure. To obtain a structural or frictional form closure grasp the object must be contained within the smaller or larger region respectively. If it is impossible to obtain a structural form closure grasp due to geometric constraints, the region is reduced to zero.

The grasped object, which is acquired using one of the above behaviors, ends up being centered at the moment of grasp because the fingers close at the same rate. In fact, this phenomenon was tested several times using the Salisbury hand. This phenomenon can be used to determine the final position of the acquired object, an important piece of information for further manipulation tasks. [Siegel 89] proposes an algorithm to identify the shape and orientation of an object using finger joint position.

Behaviors using hand and arm motion will be studied in the following sections.

3.3.3 Arm Motion Behaviors

A robotic arm is now added to the hand to enable it to manoeuvre in its surroundings. The following two approaches form the limits to the spectrum of all possible motions.

Move and Grab

1. Open the fingers to their full extent.

2. Move forward towards the object for time T at velocity V.

3. Close fingers.

The pre-image for the Move and Grab behavior, which is an extension of the pre-image for a sensorless hand without a constraining surface, is show in Figure 3.4. The pre-image is self explanatory. In Figure 3.4, L = VT, is the distance the hand moves before closing the fingers.

Move While Closing Fingers

1. Open the fingers to their full extent.

2. Move in a given direction for a length of time T while closing the fingers.

We have not presented a pre-image for this type of behavior because any general formulation of the solution would require dynamic effects to be considered, which is beyond the current scope of this work.

Many other behaviors are a combination of these two primitive behaviors. The only input is the length/time of travel which is dependent on the range of possible initial conditions. The *Move While Closing Fingers* behavior has a scooping effect, which prevents the object from squeezing away and guides the object towards the palm. If the object does not rest against a constraining surface, a combination of these two behaviors should be used; this combination consists of moving in a direction for a given length of time, and closing the fingers while maintaining the same trajectory. This behavior was implemented on a system consisting of the *Salisbury hand* and the *Puma arm* for grasping freely floating objects in space. These two types of behaviors are similar to Mason's work [85] on "Automatic Planning of Grasping".

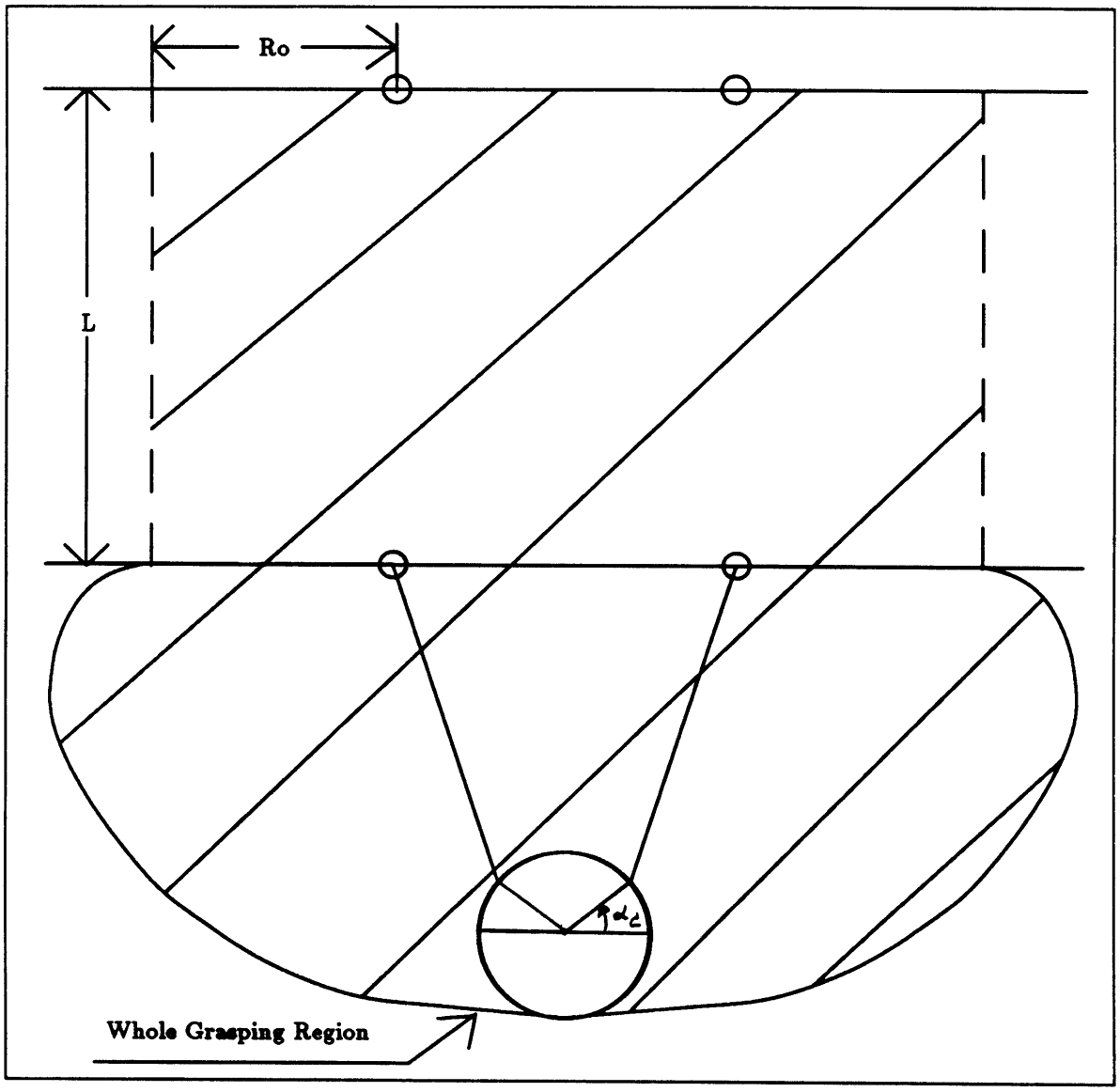

Figure 3.4: Pre-Image for Move and Grab

In this section, pre-images for sensorless behaviors have been derived with and without arm motion that guarantee grasping. As previously shown the resulting pre-images are quite limited. The next step is to examine how sensory behaviors can be used to improve the above pre-images.

3.4 Sensory Behaviors

This section examines hand behaviors when touch (simple tactile) feedback is provided. Questions such as "Is the grasping region increased with increased sensory information?" or "How can sensory information influence the design of a behavior?" are addressed in this section.

3.4.1 Grasping Region

Adding sensors to the 2-jointed model does not increase the pre-image because the hand is assumed to be fixed on a table. Even if the exact location of the object could be located using the sensory information, it would not be possible to reposition the hand to adapt for that given situation. It does not make much sense to add any sensors to a hand if it cannot be repositioned. Hence, the pre-image does not change by adding sensors to the hand. The reader is referred to the section where *Sensorless Behaviors* are discussed. The gain from having a sensor would be to indicate any failures or successes. The fingers are commanded to stop when a force is detected. This could be achieved by simply checking motor current or other sensors if they are available.

3.4.2 Arm Motion Behaviors

By adding sensors to the hand, behaviors can be designed which will increase the size of the pre-image. In fact, the pre-image is dependent on the type and amount of sensory information.

This problem is tackled by considering the simplest of all sensors: the binary sensor or binary switch. One bit of information indicates if the sensor is switched on or off (contact or no contact). This is one of the most reliable, inexpensive, and common sensors.

Approach

The procedure for determining hand behavior given sensory information is as follows:

1. The spatial distribution of the sensors on the hand is examined, and it is ensured that there are no dead zones (points on the hand without sensors which should be avoided since the hand cannot detect collisions with objects if they strike a dead zone).

2. The hand opens according to the dead zones, that is, the fingers are positioned so as to have a connected pre-image and eliminate dead zones. If the sensors cover the entire hand surface the fingers should be opened to the maximum extent. It is desirable to have the fingers fully extended because it increases the grasping region. Hence, as a design corollary a hand should have sensors on all its surfaces.

3. *Sensor Regions*, regions in which the object would be located if one of the sensors were to trigger, set a limit to where the object could be located after sensor contact.

4. A behavior will be chosen so as to reduce the size of the sensor region. The behavior depends on the sensory information and is built so as to decrease the sensor region until the area of the sensor region is equal to or smaller than the closing grasping region (which is the same as the pre-image for sensorless grasp

without arm motion). If the sensor region can be reduced to that size, the grasping of the object can be guaranteed. The following behavior is proposed:

(a) First, move the hand towards the object until any sensor triggers.

(b) Then, reposition the center of the palm above the center of the sensor region and make another approach in the same direction. Repeat the previous step until the sensor region is smaller than the closing grasping region. There are obviously infinitely many behaviors that will accomplish this task, although not all behaviors do. We are unable to prove which behavior is optimal, in the sense that it reduces the sensor region at a faster rate, but it can be shown that our behaviors accomplish this task with a small number of moves (one or two) depending on the distribution of the sensors on the hand.

(c) Finally, when the sensor region is smaller than the closing grasping region, the hand is repositioned so that the contact region is fully enclosed within the closing grasping region and trigger the behavior of chapter 3.3.1 which is simply to close the fingers.

Quasi-static motion has been assumed during the analysis, which implies that the object is not perturbed when it is touched by the hand. This assumption makes the analysis much easier but only applies if the binary sensors do not require much force to trigger relative to the mass of the grasped object or if non-contact proximity sensors are used.

A theory on how to position the fingers in order to have a continuous optimal pre-image (eliminate dead zones while maximizing the pre-image) has not been developed, but computing the ratio of the area of the connected to the disconnected pre-image gives an estimate of how well chosen the initial position of the fingers is. It is therefore possible to examine how a change in the finger position changes the relative ratio.

There is a trade-off between the shape of the pre-image and this ratio.

This analysis suggests that the number of sensors should be increased until the area of the first sensor region is less than or equal to the closing grasping region. If a hand is equipped with such sensory capabilities, one move is sufficient to locate the object and a second to acquire it. In the event that a hand is equipped with less dense sensory information, several moves are required before grasping the object.

Example

An example will illustrate the above points. Figure 3.5 shows a hand with sensory capabilities and Figure 3.6 the first sensor region for the given hand. Due to the symmetry in the location of the sensors on the fingers, the sensor regions for both fingers are identical.

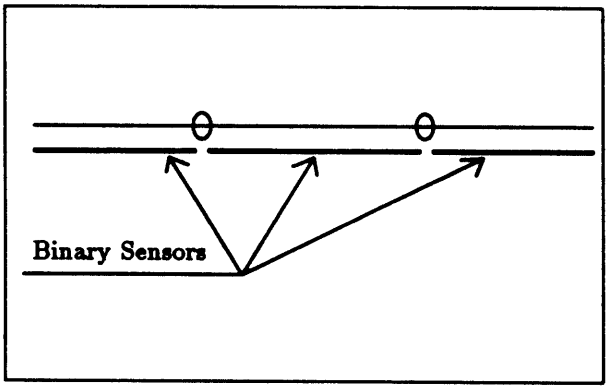

Figure 3.5: Hand and Sensors

This type of analysis shows that acquiring cylinders require only a few well distributed simple sensors on the hand's surface.

Figure 3.7 is a comparison between the size of the sensorless and sensory pre-images (assuming the entire hand surface is equipped with sensors). Adding sensory capabilities to the hand greatly increases the pre-image.

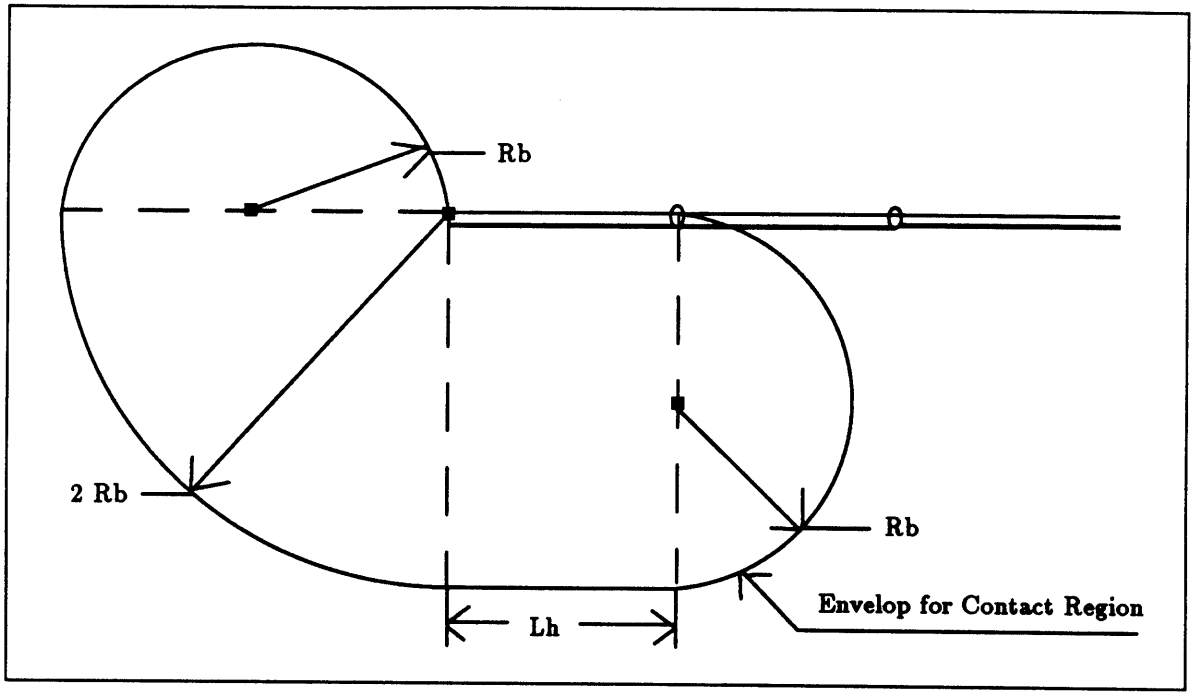

Figure 3.6: First Contact Region

3.4.3 Discussion

A simple procedure has been studied that guarantees grasping. Even though this analysis was carried out for cylinders, it can be easily extended to any other hand or any other object shape.

This would be an acceptable method for grasping massive objects in zero gravity. In fact, all that is required is to position the hand near the object's location, and initiate the reflexive grasp algorithm.

These behaviors can also be developed to search for objects. A superposition of the grasping regions will have the same effect as a guided search. A blind person proceeds in a very similar fashion when searching for an object.

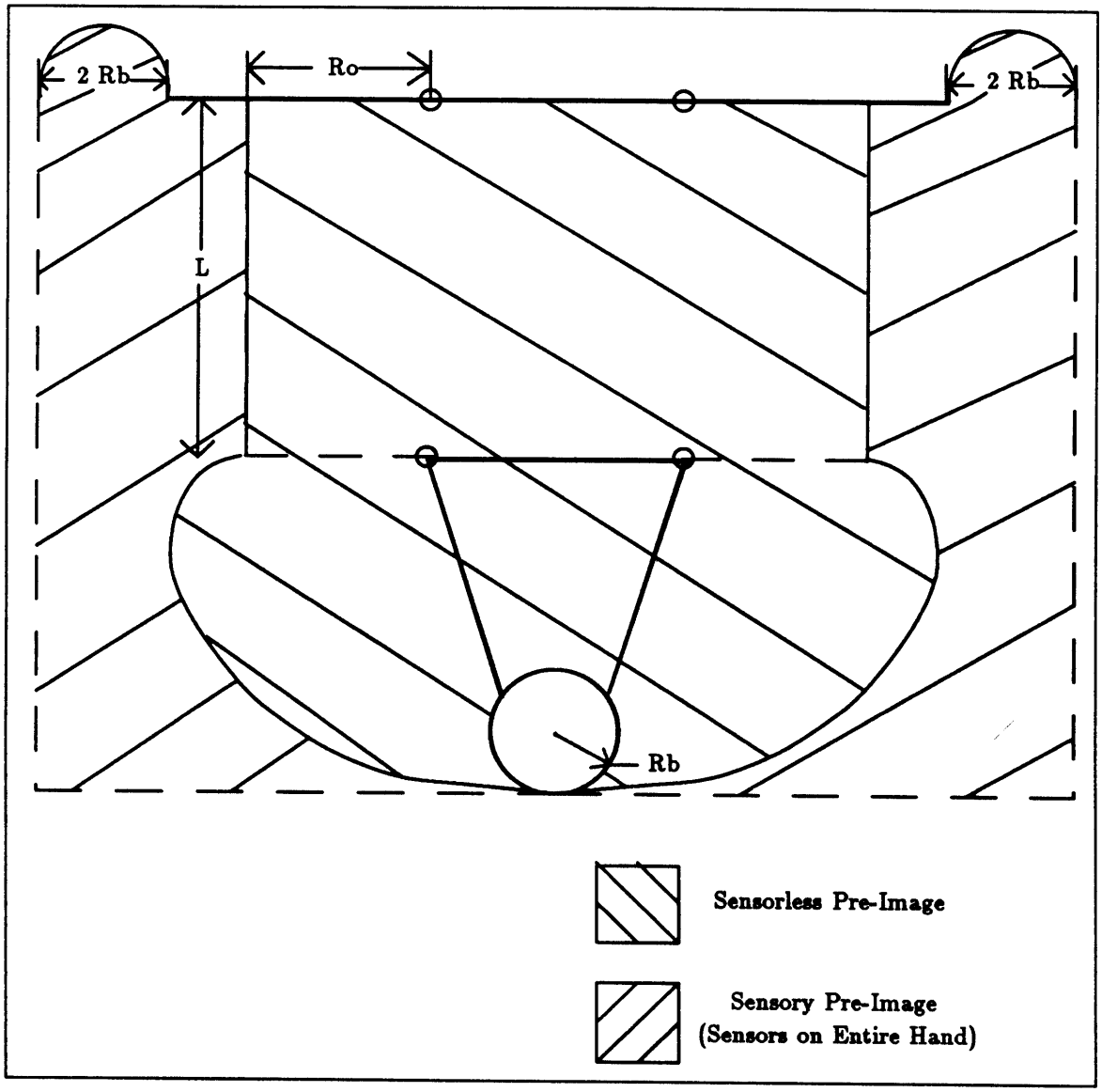

Figure 3.7: Comparison of Sensorless and Sensory Pre-Images

Chapter 4

Zero-G Grasping; 2-Jointed Hand

So far, it has been assumed that the motion of the cylinder has been dominated by frictional forces. Therefore, all the dynamic and impact effects between the cylinder and the hand have been neglected. These assumptions corresponded to quasi-static motion.

The following chapter takes a closer look at the dynamics and impact effects. This would correspond to grasping in space. Inertial forces are dominant and the only friction occurs between the hand and the grasped object.

A theoretical analysis of the dynamics between a hand and a cylinder is conducted. Then, the results of the previous analysis are used in conjunction with sensorless and sensory behaviors to derive grasping regions.

4.1 Theoretical Analysis

Two cases are examined in this section. First, equations of motion are derived for a cylinder in contact (rolling and sliding) with a finger. Then, an impact analysis is conducted to understand the cylinder's motion in between impacts.

4.1.1 Equations of Motion During Contact

Equations of motion for three specific cases are examined. The common assumptions to all cases is that the cylinder moves on a frictionless surface, and that the fingers close at a constant angular velocity. In the first case it is assumed that the hand has frictionless fingers, in the second case it is assumed that there is enough

friction so that the cylinder rolls without sliding on the finger, and in the third case it is assumed that the contact forces fall outside the friction cone so that the cylinder slides along the finger. The first analysis is a particular case of the third.

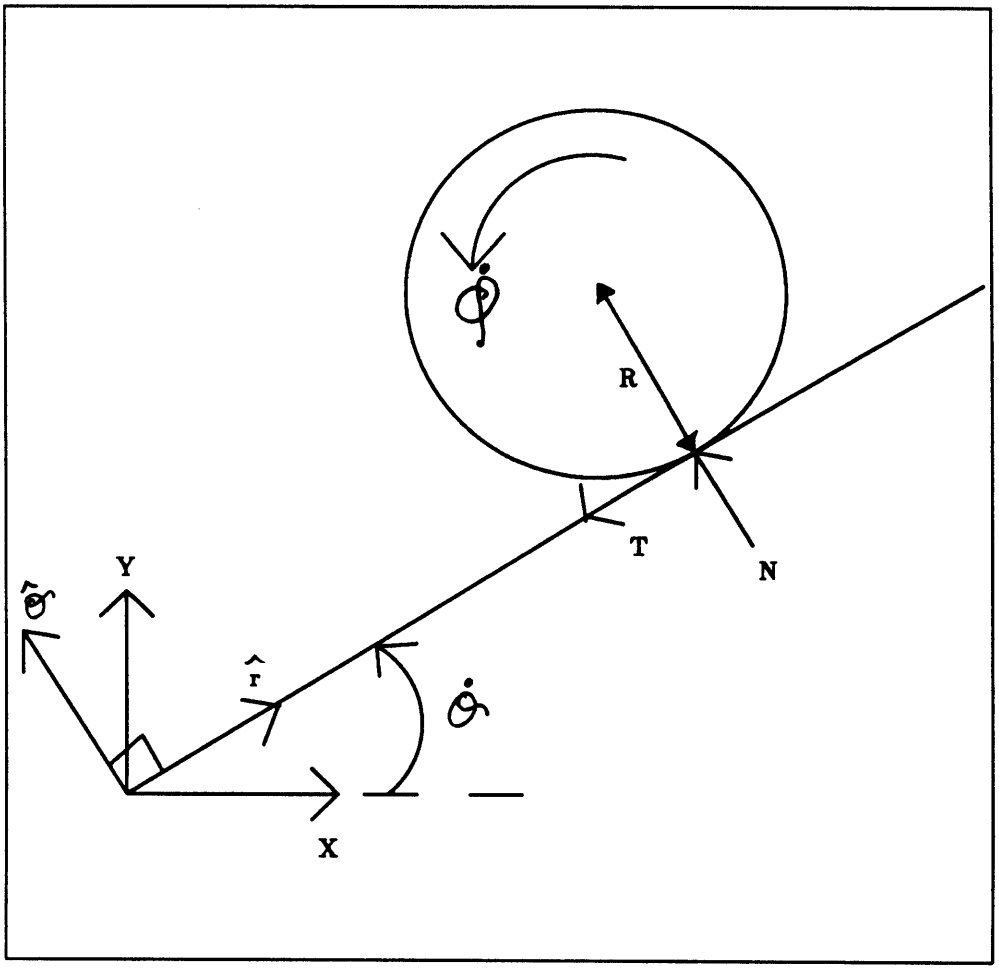

Figure 4.1: Zero-G Coordinate System

The following terms are used during this analysis:

1. $\dot{\theta}$: The angular velocity of the finger.

2. $\dot{\phi}$: The angular velocity of the cylinder.

3. R : The radius of the cylinder.

4. t: time.

5. r(t) : The radial position of the cylinder on the finger function of time.

6. r_0 : The radial position of the cylinder on the finger at time t=0.

7. $\dot{r}$: The translational velocity along the finger.

8. N : The normal contact force between the finger and the cylinder.

9. T : The tangential contact force between the finger and the cylinder.

10. m : The cylinder's mass.

11. μ : The friction coefficient.

A reference frame along with some other variables are defined in Figure 4.1.

The equations of motion for a cylinder in contact with a frictionless finger (this corresponds to case 1) are needed to construct grasping regions. It will be shown that the radial position of the cylinder along the finger at the contact point as function of time is equal to:

$$r(t) = r_0 \cosh(\dot{\theta} t) \tag{4.1}$$

The equation of motion of the cylinder for the second case (rolling of the cylinder on the finger) is:

$$r(t) = r_0 \cosh\left(\dot{\theta} t \sqrt{\frac{2}{3}}\right) \tag{4.2}$$

The equation of motion for the third case (sliding of the cylinder on the finger) is:

$$r(t) = C_1 \exp(M_1 t) + C_2 \exp(M_2 t) - \mu R \tag{4.3}$$

With:

$$\begin{aligned} M_1 &= \dot{\theta}(-\mu - \sqrt{\mu^2 + 1}) \\ M_2 &= \dot{\theta}(-\mu + \sqrt{\mu^2 + 1}) \end{aligned} \tag{4.4}$$

C_1 and C_2 are constants of integration. It should be noticed that $M_1 < 0$ and $M_2 > 0$, and that case 1 corresponds to case 3 when $\mu = 0$.

This analysis indicates that the cylinder will move along the finger at an exponential rate. This result discourages the design of a grasping behavior that will use the sliding motion of the cylinder along the finger to develop a pre-image. If such a behavior is wanted the above equations can be used to derive the grasping region. Impact equations shall be examined next in light that they will provide grounds for developing a behavior to grasp cylinders in a zero-g environment.

4.1.2 Equations of Motion During Impact

Figure 4.2 will be referred to for the rest of this analysis. A rotating coordinate reference frame is located at the joint of the finger.

The following terms need to be defined:

1. $\dot{\theta}$: The angular velocity of the finger.

2. V_b : The magnitude of the translational velocity of the cylinder before impact.

3. $V_b n$: The normal component of V_b.

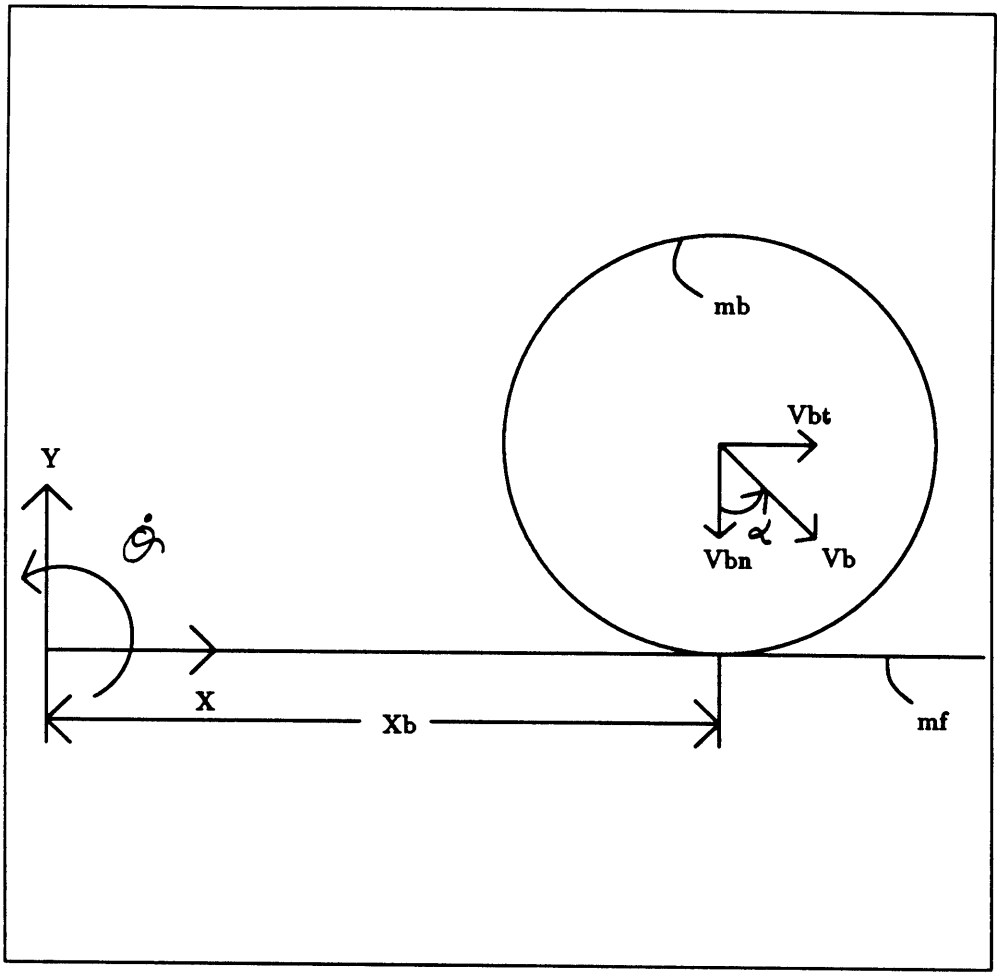

Figure 4.2: Impact Diagram

4. V_bt : The tangential component of V_b.

5. α : The incident angle of velocity V_b.

6. l_f : The length of the finger.

7. m_f : The mass of the finger.

8. m_b : The mass of the cylinder.

9. X_b : The distance from the reference to the impact point.

10. e : The coefficient of restitution.

The (') symbol will be used to denote the time interval after impact. For example V_b' will be the translational velocity of the cylinder after impact.

The two bodies are assumed to have frictionless contact. Using conservation of linear and angular momentum it can be shown that the cylinder's velocity after impact is equal to:

$$V_b' = \frac{m_f l_f^2(1+e)X_b\dot{\theta} - (3X_b^2 m_b \cos(\alpha) + m_f l_f^2 e\cos(\alpha)V_b)}{m_f l_f^2 + 3X_b^2 m_b} \tag{4.5}$$

If the angular velocity of the finger is assumed to remain unchanged after impact (ie the finger is infinitely massive) then the above expression can be greatly simplified to:

$$V_b' = (1+e)X_b\dot{\theta} - e\cos(\alpha)V_b \tag{4.6}$$

The infinite mass assumption will increase the transfer of energy during impact, and hence increase the cylinder's exit velocity. Other implications of this assumption will be discussed in Chapter 6. These impact results will be used to develop grasping regions for the following behaviors.

4.2 Sensorless Behaviors

This first class of behaviors involves no sensors. They are the simplest of behaviors but necessary to consider because they provide conservative answers and grounds to prove the success of certain grasping behaviors.

4.2.1 Grasping Region

The impact velocity of the cylinder and the coefficient of restitution cannot be measured due to the lack of sensing. We therefore make the following assumptions.

First, the coefficient of restitution is chosen equal to one (conservative); second, the cylinder is assumed to be at rest (ie. $V_b = 0$). It should be noted that the coefficient of restitution is hard to measure because it is function of material properties, impact velocities, shape, and size.

Having made these these assumptions V_b' can be further simplified to:

$$V_b' = 2X_b\dot{\theta} \tag{4.7}$$

Only structural form closure grasps are considered because the fingers were assumed to be frictionless in the impact analysis. In order to solve for the grasping region, the motion of the cylinder between impacts is needed. General equations describing the motion will be derived.

All the symbols are defined in Figure 4.3. The following equations describe the motion of the cylinder between any two consecutive impacts. Again, the (') symbol will be used to refer to conditions after impact. L_1 : is the distance traveled by the cylinder in between impacts.

$$\begin{aligned} \theta &= \frac{\dot{\theta_1}}{V_b} L_1 \\ L_1 &= \frac{R_b - R_b\cos(\theta) - R_b\tan(\theta)\sin(\theta) - X_2\tan(\theta)}{\cos(\alpha)\tan(\theta) - sin(\alpha)} \\ X_2' &= \frac{X_2 + L_1\cos(\alpha) + R_b\sin(\theta)}{\cos(\theta)} \end{aligned} \tag{4.8}$$

Thus far, the location of the second impact has been determined, but the cylinder's velocity after impact remains undetermined.

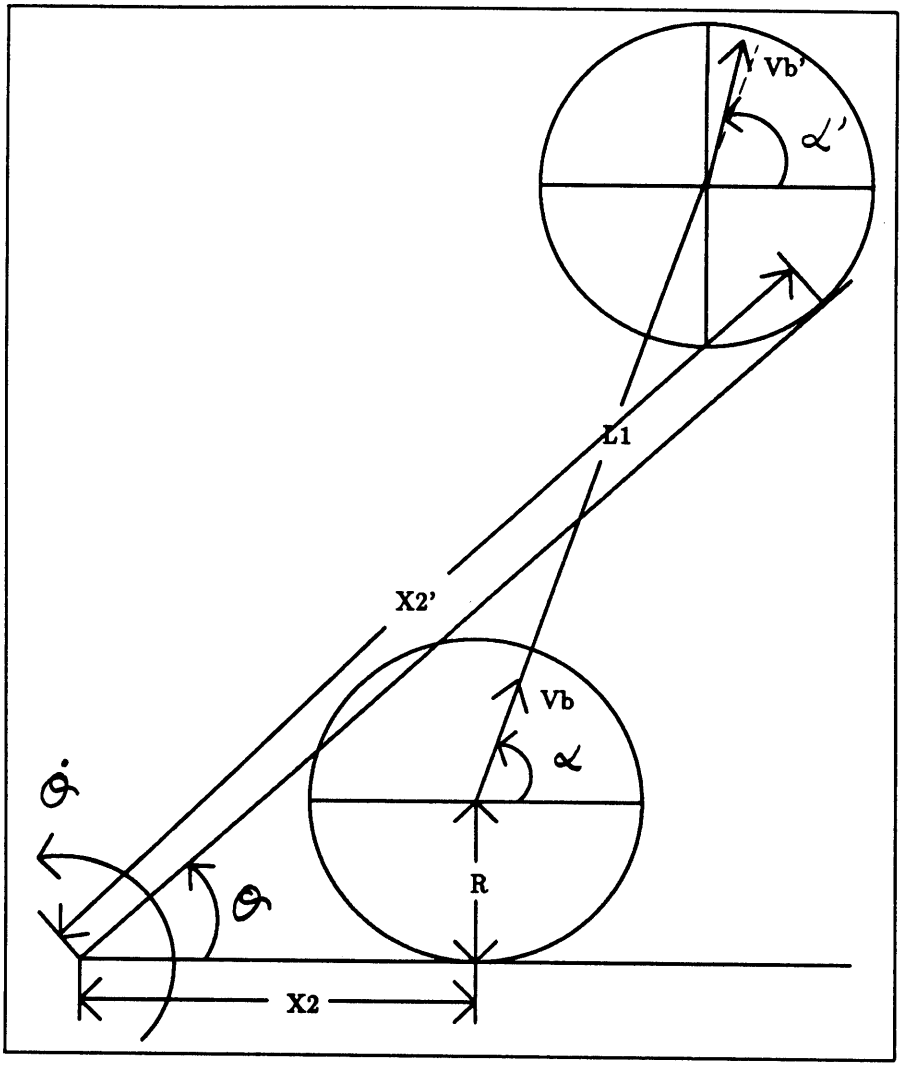

Figure 4.3: Cylinder's Motion In Between Impacts

The equations describing the cylinder's velocity after impact are as follows:

$$
\begin{aligned}
V_b' &= \sqrt{[2\dot{\theta}_1 X_2' + V_b \sin(\alpha - \theta)]^2 + V_b^2 \cos(\alpha - \theta)^2} \\
\alpha' &= \arctan\left(\frac{2\dot{\theta}_1 X_2' + V_b \sin(\alpha - \theta)}{V_b \cos(\alpha - \theta)}\right)
\end{aligned}
\tag{4.9}
$$

These equations can be applied recursively to compute the locations of all impacts.

The grasping region has been developed for the case where the cylinder will impact the hand no more than twice. This is somewhat an arbitrary decision but is justified by the fact that this reduces the error in prediction and that two impacts would have given the finger a closing motion of about 90°.

The grasping region is constructed using the following iterative procedure:

1. Pick an X_2.
2. Solve for θ and X_2' using equations(4.8).
3. Solve for V_b' and α' using equations(4.9). This would describe the the state after the second impact.
4. Use θ, X_2', and α' in conjunction with equation (4.8) to compute the state of the system after the third impact. The states after third impact will be denoted by (").
5. If X_2" is greater than the finger's length decrease X_2 else increase X_2.
6. Reiterate process starting at step 1 till X_2" is equal the finger length.

The above algorithm will eventually converge and provide the three contact points for the given three impacts which when connected define the contact grasping region. The three points are defined as follows:

$$R_0 = X_2 \;\; ; \;\; \theta_0 = \pi - \theta_1 - \theta_2 - \arccos\left(\frac{D_h - R_h}{L_h}\right)$$

$$R_1 = X_2' \;\; ; \;\; \theta_1 = \theta$$

$$R_2 = X_2'' \;\; ; \;\; \theta_2 = \theta'$$

The whole and center grasping regions can be constructed by using a simple change of coordinates. The reader is referred to chapter 3 for an example on this method. The following section will provide a concrete example of such an algorithm.

4.2.2 Example

The zero-G pre-image defined above is shown in Figure 4.4 using the following dimensions for the hand and cylinder:

$D_h = 6.0$; $L_h = 24.4$; $R_b = 3.8$

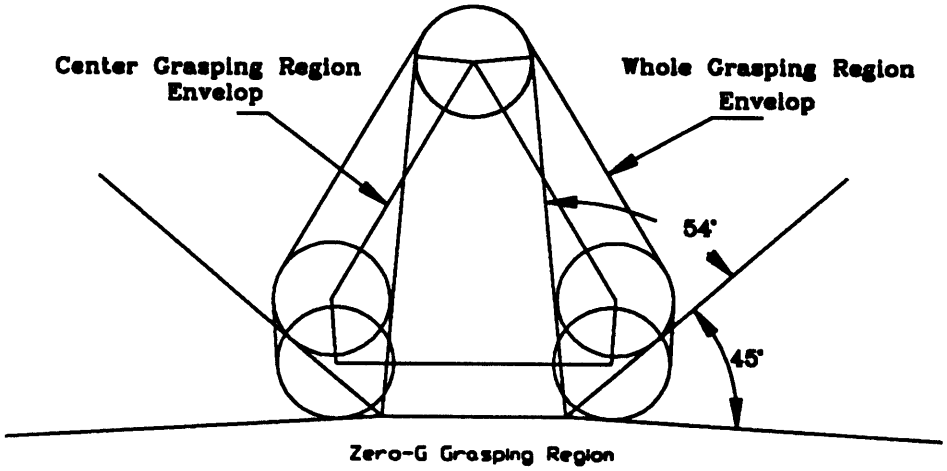

Figure 4.4: Zero-G Grasping Pre-Image for a Sensorless Hand

The construction points are as follows:

$$R_0 = 2.8 \ ; \ \theta_0 = -3.6°$$

$$R_1 = 7.7 \ ; \ \theta_1 = 45°$$

$$R_2 = 24.4 \ ; \ \theta_2 = 53.7°$$

The whole and the center grasping regions are shown in Figure 4.4.

4.3 Sensory Behaviors

This section looks at how sensory information affects grasping behaviors. Different behaviors will be analyzed as a function of the sensory information available to detect

changes in the environment. Three types of sensors are considered: a one-bit contact sensor, a force sensor, and a position sensor such as a vision system. The general strategy in developing these behaviors will be to reduce the impact forces using the provided sensory information.

4.3.1 Matching Velocities

This behavior consists of matching the velocity of the hand with that of the cylinder. Here, the strategy consists of matching the hand's trajectory with that of the cylinder. A vision system can be used to track the cylinder's trajectory. Then the problem is reduced to enclosing the cylinder inside the sensorless grasping region which was derived earlier. As long as the cylinder is fully enclosed within the grasping region, the behavior of closing the fingers will ensure the acquisition of the cylinder. This type of behavior can deal with uncertainty in sensing the cylinder's position. It is a sufficient condition that the position error be enclosed within the grasping region. Hence, the grasping region sets an upper limit on the allowable position error.

The advantage of such a behavior is the minimization of impact forces. But this behavior can run into some limitations in cases where the cylinder is moving at high velocities. In fact, the robot hand might reach its workspace limits very quickly. Another issue here is the actuator dynamics; in fact the actuators might not be able to provide enough torque to match the desired trajectory.

4.3.2 Reducing Impact forces

Much research has been devoted to analyzing and to modeling of impact forces. Johnson[58] has developed a method for estimating impact forces based on momentum and energy principles. The predicted impact forces using the Johnson model closely matched the experimental forces when at least one of the contacting surfaces has a low stiffness. Kahng and Amirouch[87] extended the Johnson model by incor-

porating the energy loss due to structural damping. Kahng's model was somewhat more accurate in predicting peak impact forces; but both of these methods failed to predict peak impact forces for high spring constants. The outcome of these papers is that a relatively simple model is adequate in predicting impact forces which can be minimized by using low stiffness materials.

Others, like Parker[85] were more interested in reducing impact forces during robot manipulation. He implemented on a two-degree-of-freedom robot hand a control algorithm very similar to a "bang bang" controller to reduce impact forces. The basic idea was to accelerate the finger with a maximum control signal. Then, apply the full negative control to stop the finger as it reaches the object to be grasped. But in this case the objects were assumed to be stationary. The problem of interest to us is the grasping of moving objects. Similar control algorithms as outlined by Wang[89] or Buhler[89] can be developed for grasping moving objects.

Wang[89] looks at the problem of catching a circular disk moving on a smooth surface using a paddle. He proposes two alternatives to catching the disk. A sinusoidal and a quadratic paddle motions are analyzed, and shown to be feasible in simulation. Buhler, Koditschek, and Kindelmann[89] have analyzed and tested control algorithms for catching pucks sliding on a vertical surface. They have succeeded in the "catching" task using a "mirror" algorithm because their "grasps" rely on gravity forces to maintain contact, they are force-closure grasps.

Such algorithms are suitable for implementation on a robot hand; but it is also of interest to develop grasping behaviors that are specific to sensory information.

One alternative is to use the one bit sensor. If placed in key locations this can in fact be of some use. The sensor would have to be located on the palm. The behavior associated with such a sensor would be to close the fingers as soon as the sensor was triggered. Due to physical limitations such as actuator dynamics, such a sensor should not be placed on the fingers, because the time response of the robot hand

would have to be extremely fast. And also the finger's motion would also perturb the cylinder's trajectory.

Another alternative would be to use a force sensor. The first solution that comes to mind would be to use the force at the contact as an input to a controller that would in turn actuate the hand so as to reduce the impact forces. Such a control algorithm would require extensive modeling of the rigid bodies and the drive system. Eppinger[88] showed that the dynamics between the actuator and the sensor contribute to instabilities in force control manipulations. Sundaram[90] has shown that stable force and position control can be achieved using joint torque feedback in conjunction with endpoint force feedback.

To conclude this section, two main points should be kept in mind. First, a soft material should be used on the hand to reduce impact forces. Second, sensors tracking the cylinder's state at times before impact should be used (ie. vision system) because sensory information concerning the state of the cylinder at impact being very difficult to obtain in reality.

Chapter 5

Extension to a 4-Jointed Hand

The analysis in the previous chapters analyzed grasping behaviors as related to a 2-jointed hand. A 4-jointed hand, two fingers and two joints per finger presented in Figure 5.1 , is now considered. L_1, and L_2 correspond to the finger's second and first link respectively, and L_3 to the wrist. Concepts presented in the previous chapters apply to this model as well, but we present extensions possible with this model in this chapter. The first section examines conditions for grasping . A theoretical analysis demonstrating the hand preshape required for sliding a cylinder in a circular path, is then presented. The theoretical results are used in subsequent sections for designing appropriate behaviors.

5.1 Necessary Conditions for Grasping

Necessary conditions for grasping need to be specified before the design of any behavior. Actually, these conditions can also be viewed as an intrinsic part of each behavior. Each behavior would first check whether a cylinder is graspable at all even before attempting to grasp it.

5.1.1 Necessary Conditions For Grasping

Establishing necessary conditions (ie. finding the maximum cylinder size that can be grasped given a hand geometry) for grasping is not a simple task, and a closed form solution does not exist. Numerical results have been generated and presented using contour plots.

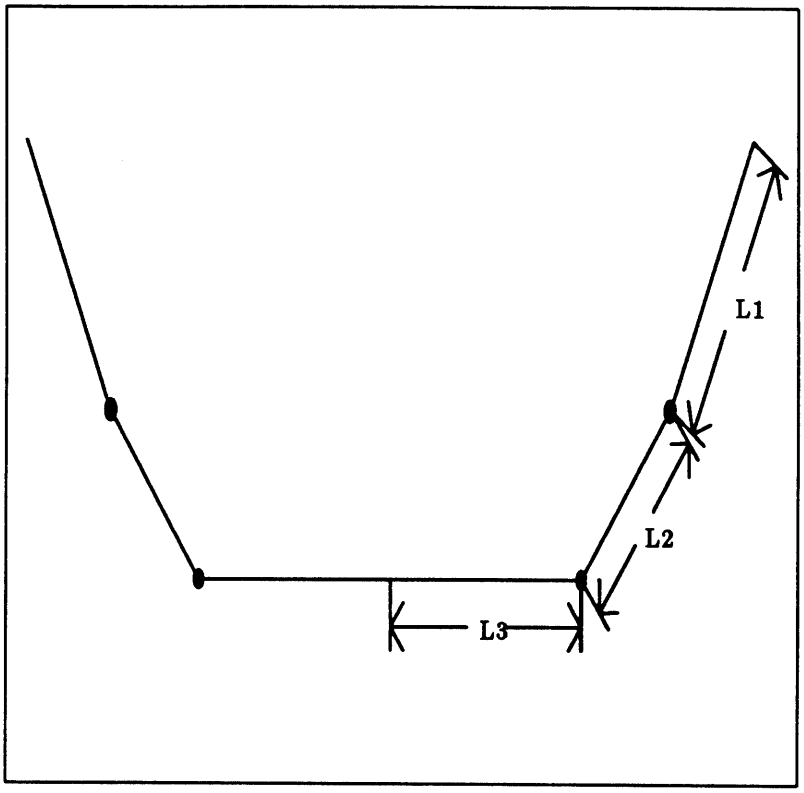

Figure 5.1: 4-Jointed Hand

The following assumptions and conjectures are made during the analysis:

1. Only structural form closure grasps are considered, because they are more secure grasps, and do not require any knowledge about the friction between the hand and the grasped object.

2. The final grasp will be symmetrical due to the symmetries within the hand structure and the cylinder.

3. Structural form closure requires at least three contact points between the hand and the cylinder. Therefore there are only four possible combinations of grasps. The four grasps consist of link (1,2); (2,3); (1,3); and (1,2,3). The combination

(1,2) refers to a grasp when link L_1, and L_2 make contact. These four combinations will be referred to as case 1, case 2, case 3, and case 4, respectively. The general solution to the problem is obtained by taking the maximum of each of the four cases. It should be noted that case 2 is equivalent to the 2-jointed hand model. Figure 5.2

Given the dimensions of the finger lengths (L_1, L_2, and L_3) an optimal cylinder radius was computed for each of the four cases using a algorithm that searched for the largest cylinder that can be grasped given a specific hand dimensions. To cover all possible combinations of link length ratios the following dimensionless ratios have been defined:

$$L_1^* = \frac{L_1}{L_1 + L_2 + L_3}$$

$$L_2^* = \frac{L_2}{L_1 + L_2 + L_3}$$

$$R^* = \frac{R_{max}}{L_1 + L_2 + L_3}$$

R_{max} is the maximum graspable cylinder given L_1^* and L_2^*. Each pair of L_1^* and L_2^* defines a point in the plane which in turn determines a hand geometry for a given L_3. This dimensionless operation maps the whole domain to a square, with L_1^* and L_2^* bounded between one and zero. Moreover, the sum of L_1^* and L_2^* has to be less than or equal to one. This further restricts the domain of all possible link combinations to a triangle defined by the the following three points: (0,0), (1,0), and (0,1).

The results for each case are shown in Figure 5.3, Figure 5.4, Figure 5.5, and Figure 5.6. The general solution, shown in Figure 5.7, is obtained by taking the maximum of the four cases.

The regions outside the contour lines are equivalent to no solutions. The contour plot for case 1 shows two maximums located around the points (0.25,0.6) and (0.48,0.25).

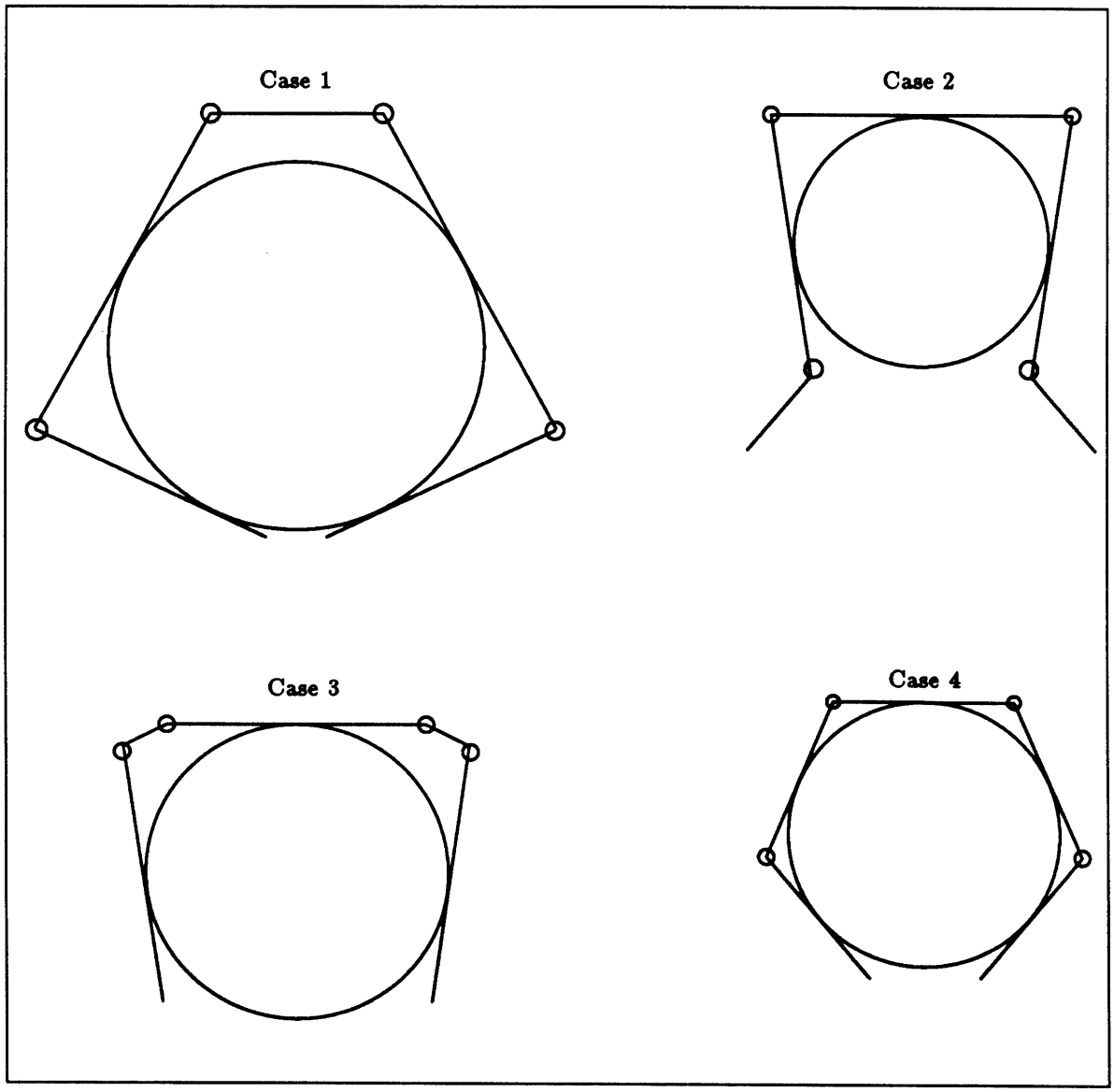

Figure 5.2: Four Possible Structural Form Closure Grasps

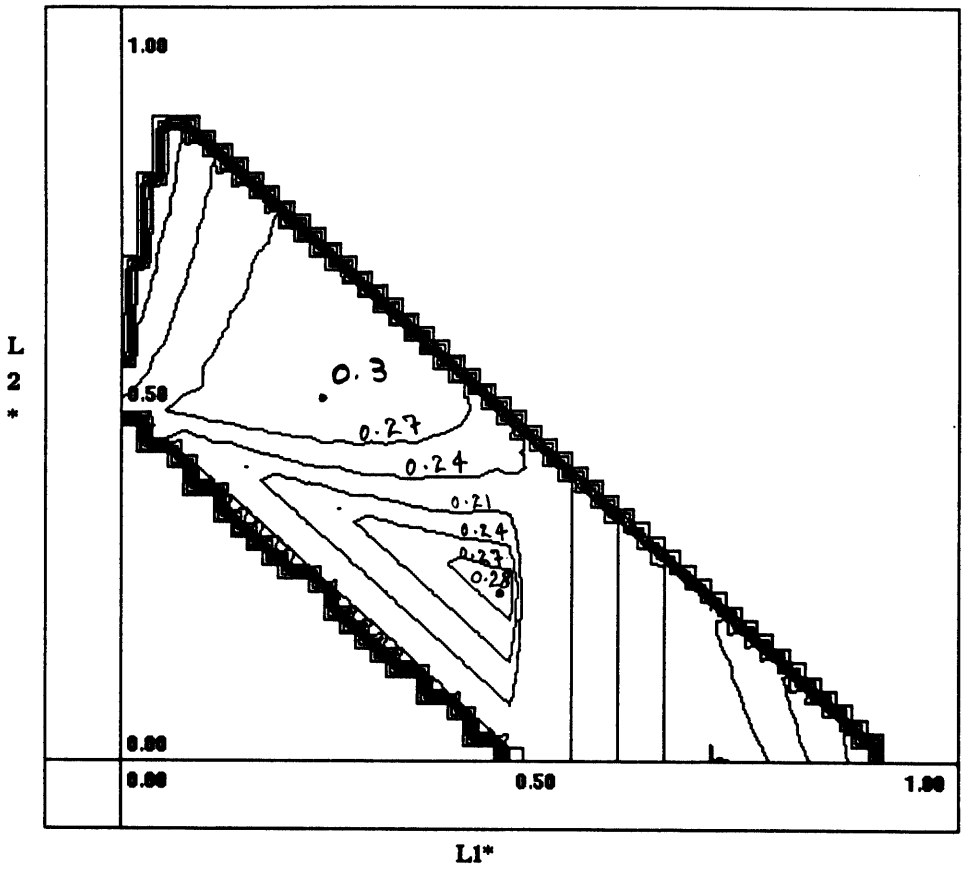

Figure 5.3: Maximum Dimensionless Radius R^* for Case 1

Figure 5.4 displays a maximum at (0.0,0.5) This is not surprising because in this case link 1 does not play any role in the grasp; and therefore the maximum occurs when the length of the third link is equal to zero.

Figure 5.5 displays a maximum at (0.25,0.49). The other maximums that appear are due to numerical sensitivity. The solution is very sensitive to numerical computations. The solution is sensitive because of the inherent nature of the problem. The numerical solution is basically looking for intersections between lines and circles. It

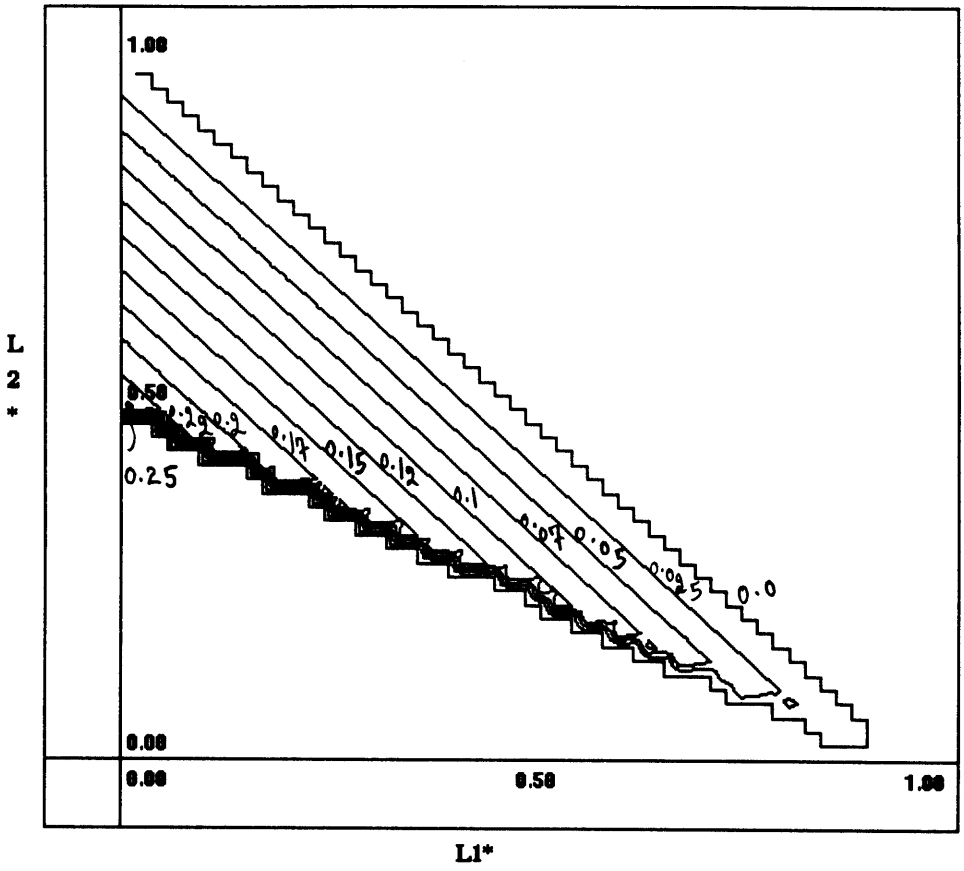

Figure 5.4: Maximum Dimensionless Radius R^* for Case 2

should be noted that the solution goes abruptly to zero near the border lines. This is indicative that a hand design should be avoided around these regions due to the sensitivity in the initial conditions.

Figure 5.6 displays four maximums at approximately (0.15,0.5), (0.2,0.5), (0.25,0.5), and (0.3,0.5). These four maximums appear because of numerical sensitivity. As will be shown in the following section there is only one maximum.

It is necessary to note that the contour plots display the ratio of the maximum

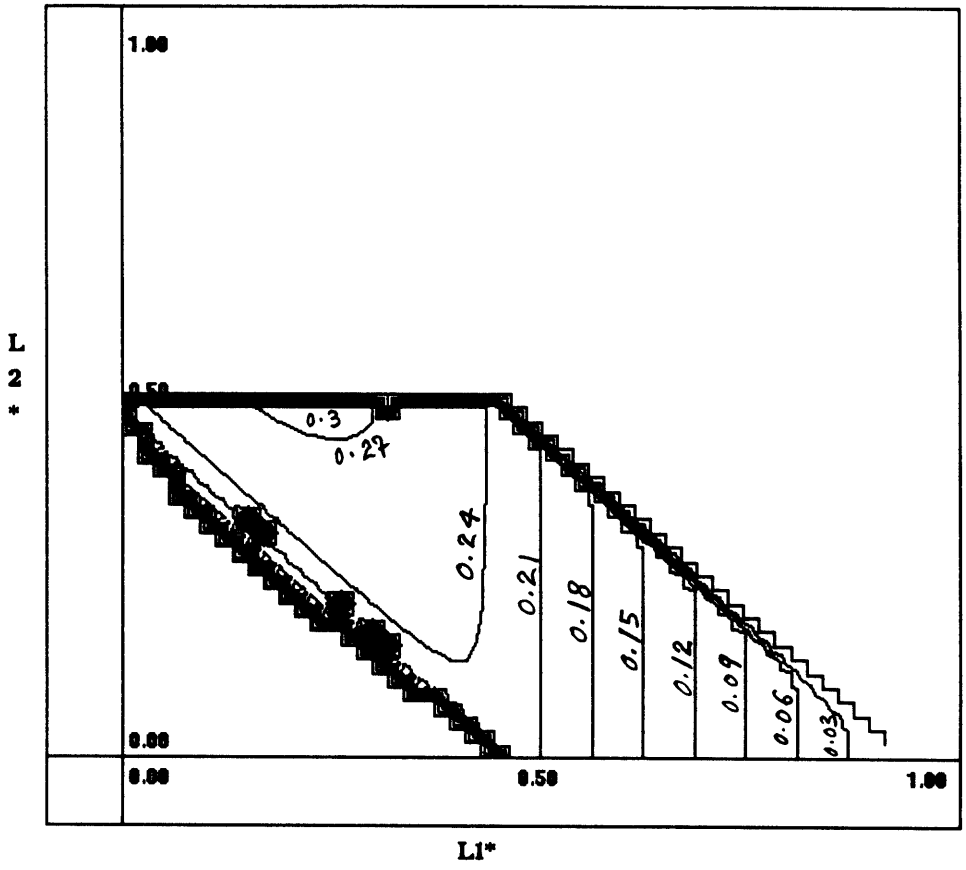

Figure 5.5: Maximum Dimensionless Radius R^* for Case 3

cylinder to the hand size. This is a relative measure and could be used in designing hands. The peaks on the contour plots correspond to cases of hands being able to grasp large cylinders relative to their dimension. This information could be used when dimensioning a hand.

Figure 5.7 shows that the maximum occurs somewhere around the point (0.25,0.5). The following section looks at the problem of designing a 4-jointed hand that can grasp the largest cylinder relative to its size; and comparing the result with the

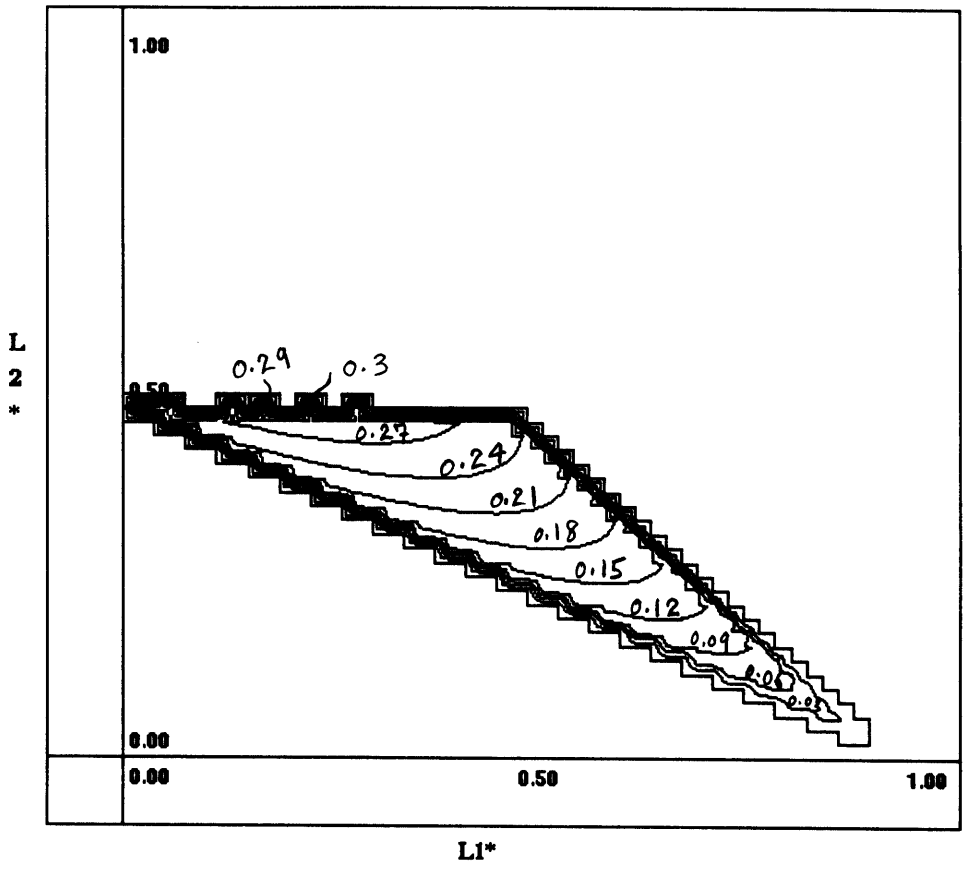

Figure 5.6: Maximum Dimensionless Radius R^* for Case 4

theoretical minimum.

5.1.2 On hand designs

Following the discussion from the previous section, we show how to design a hand that can grasp the largest cylinder relative to its size using a structural form closure grasp. Three types of hand geometries will be considered; the theoretical minimum, the 2-jointed hand, and the 4-jointed hand respectively.

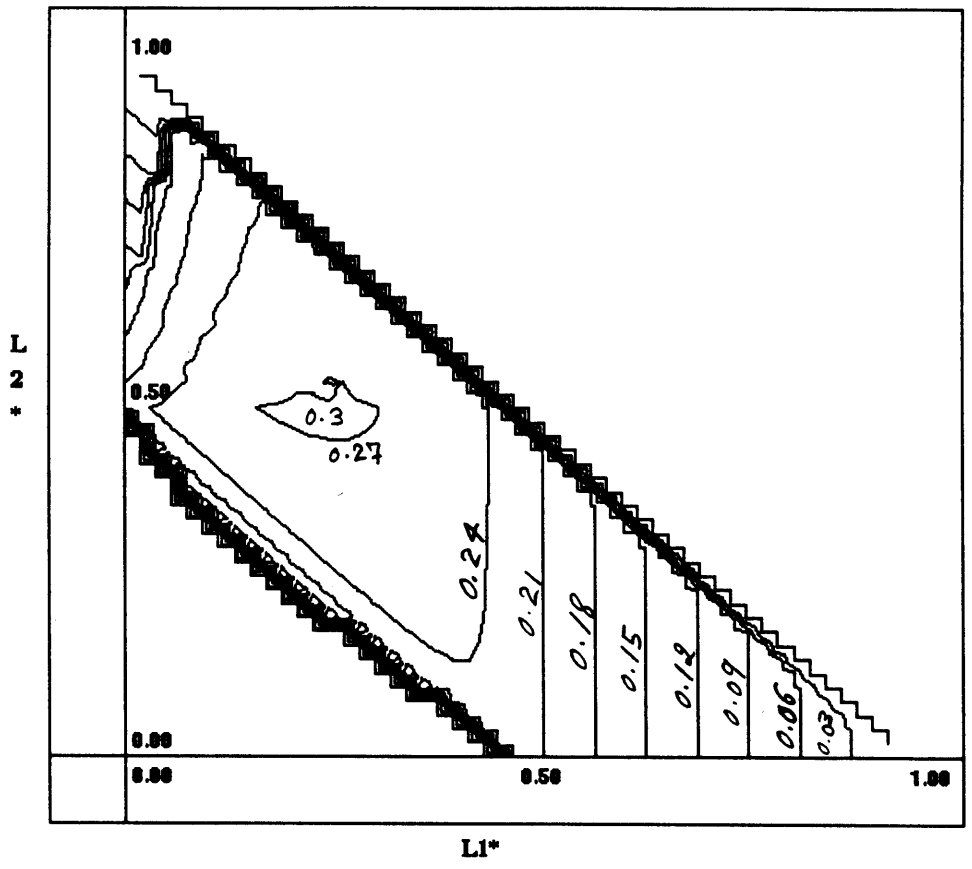

Figure 5.7: Maximum Dimensionless Radius R^* of All Four Cases

It can be shown that the smallest hand that can grasp a cylinder of radius R, has total length $L_{Theoretical}$:

$$L_{Theoretical} = \pi R$$

Such a hand would be composed of an infinite number of infinitely small links. The shape of such a hand is a semi circle. It wraps half way around the cylinder.

For a 2-jointed hand the minimum occurs when the finger length is equal to the

wrist length (ie. $L_H = D_H$ or $L_1 = 0; L_2 = L_3$). For this geometry, the total hand length is:

$$L_{2-jointed} = 4R$$

For a 4-jointed hand the minimum occurs when :

$$L_1 = L_3 = \frac{L_2}{2}$$

For this geometry, the total hand length is:

$$L_{4-jointed} = 8(\sqrt{2} - 1)R$$

The dimensionless ratios (L_1^* and L_2^*) corresponding to this geometry are:

$$\begin{aligned} L_1^* &= 0.25 \\ L_2^* &= 0.50 \end{aligned}$$

Hence, explaining the maximum in each of the contour plots.

It is interesting to look at the following ratios:

$$\frac{L_{Theoretical}}{L_{2-jointed}} = \frac{\pi}{4}$$

$$\frac{L_{Theoretical}}{L_{4-jointed}} = \frac{\pi}{8(\sqrt{2} - 1)}$$

The ratio $\frac{L_{Theoretical}}{L_{2-jointed}}$ is approximately 0.78 and the ratio $\frac{L_{Theoretical}}{L_{4-jointed}}$ is approximately 0.94. Consequently, the 4-jointed hand is 94% close to the theoretical minimum,

which could be used as an argument for not adding more finger joints. Other factors, of course, must also be taken into account when designing hands.

A scaled drawing of these hands is shown in Figure 5.8.

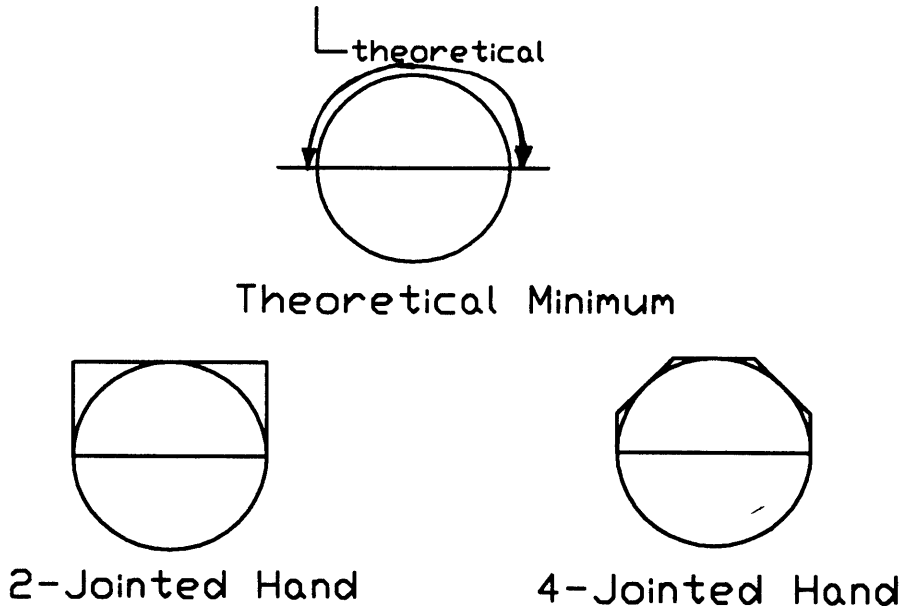

Figure 5.8: Optimal Geometries for Hands

5.2 Quasi Static Grasping Region

Pushing operations for the 4-jointed hand are now considered. A theoretical derivation on the hand preshape needed to push a cylinder in a circular path is first presented. Then, a behavior is designed using the results from the analysis.

5.2.1 Theoretical Analysis and Assumptions

Given a hand with two fingers (each finger with two links), it is of interest to find the hand preshape that will maintain the motion of a cylinder in a circular path. The

angle between the first and second link is kept fixed. Only the first link is allowed to rotate about its joint.

An expression for the angle between the first and the second link as a function of the given parameters will be derived in the following derivation. We will proceed by computing the velocity of a point on the cylinder due to the rotation of the first link. This velocity vector will provide the direction of the frictional force which will be used to sum the moments exerted on the cylinder.

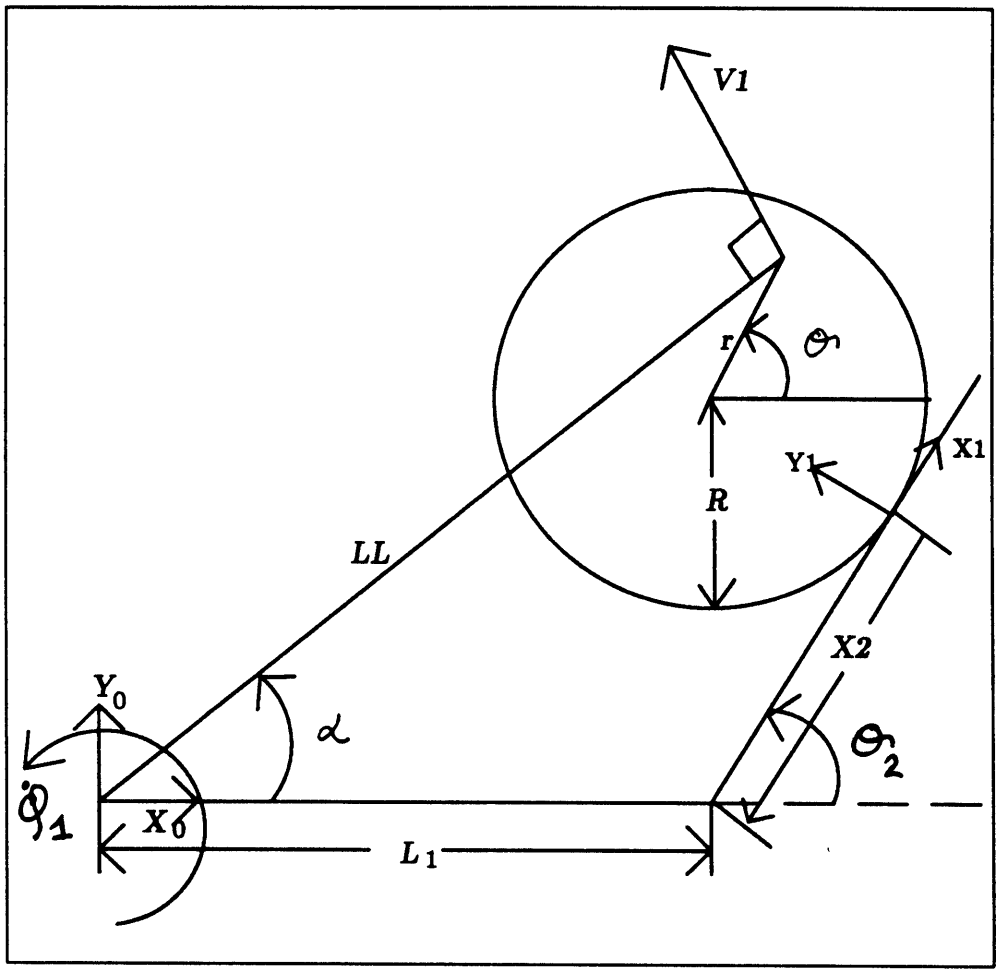

Figure 5.9: Notation

The following terms are used throughout the derivation:

1. V_0 : The velocity of a point on the cylinder due to the rotation of the first link. The subscript (0) refers to the coordinate system at (x_0,y_0). Similarly, the subscript (1) refers to the coordinate system at (x_1,y_1).
2. df : The differential force at any point on the cylinder.
3. dm : The differential moment due to the differential force.
4. M : The total moment on the cylinder.
5. L_1 : The length of the first link.
6. LL : Distance between reference frame to a point on the cylinder.
7. $\mu(r,\theta)$: The friction coefficient.
8. $P(r,\theta)$: The pressure distribution function under the cylinder.
9. R : Radius of the cylinder
10. r : Distance from the center of the cylinder to a point on the cylinder.
11. X_2 : The distance between the second joint and the contact point between the cylinder and the second link.
12. θ_2 : The angle between the first and second link.

The other symbols are defined in Figure 5.9.

V_0 is equal to:

$$V_0 = \dot{\phi}_1 LL \begin{bmatrix} -\sin(\alpha) \\ \cos(\alpha) \end{bmatrix} \tag{5.1}$$

Substituting for α, V_0 becomes:

$$V_0 = \dot{\phi}_1 \begin{bmatrix} -(X_2 \sin(\theta_2) + R\cos(\theta_2) + r\sin(\theta)) \\ L_1 + X_2\cos(\theta_2) - R\sin(\theta_2) + r\cos(\theta) \end{bmatrix} \tag{5.2}$$

V_1 is found by transforming V_0 to the (x_1,y_1) coordinate system:

$$V_1 = \dot{\phi}_1 \begin{bmatrix} -R + L_1\sin(\theta_2) - r(\sin(\theta)\cos(\theta_2) + \cos(\theta)\sin(\theta_2)) \\ X_2 + L_1\cos(\theta_2) + r(\sin(\theta)\sin(\theta_2) + \cos(\theta)\cos(\theta_2)) \end{bmatrix} \tag{5.3}$$

The frictional force at each point has a direction opposite to the velocity vector. The differential moment due to each differential force is equal to the cross product of the position vector and the frictional force vector:

$$dm = \begin{bmatrix} r\cos(\theta - \theta_2) \\ (R + r\sin(\theta - \theta_2)) \end{bmatrix} \times df \tag{5.4}$$

$$dm = \begin{bmatrix} r\cos(\theta - \theta_2) \\ (R + r\sin(\theta - \theta_2)) \end{bmatrix} \times \left[\mu(r,\theta)P(r,\theta)\frac{-V_1}{\|V_1\|} r\, dr\, d\theta\right] \tag{5.5}$$

After cross multiplying the above equation and integrating over the whole area of the cylinder, the total moment on the cylinder was found to be:

$$M = \int_0^R \int_0^{2\pi} [r(Y_1 r\cos(\theta - \theta_2) - X_1(R + r\sin(\theta - \theta_2)))] \frac{-\mu(r,\theta)P(r,\theta)}{\|V_1\|} d\theta\, dr \tag{5.6}$$

with:

$$\begin{aligned} X_1 &= -R + L_1\sin(\theta_2) - r(\sin(\theta)\cos(\theta_2) + \cos(\theta)\sin(\theta_2)) \\ Y_1 &= X_2 + L_1\cos(\theta_2) + r(\sin(\theta)\sin(\theta_2) + \cos(\theta)\cos(\theta_2)) \end{aligned} \tag{5.7}$$

The pressure distribution and the friction coefficient are assumed to be uniform under the cylinder. After simplifying the above expression, the above integral can be reduced to:

$$M = \mu \frac{mg}{\pi R^2} \int_0^R \int_0^{2\pi} - \frac{r(Y_1 r \cos(\theta - \theta_2) - X_1(R + r \sin(\theta - \theta_2)))}{\sqrt{X_1^2 + Y_1^2}} \, d\theta \, dr \qquad (5.8)$$

The problem is now reduced to finding the angle θ_2 that will reduce the integral to zero, and hence set the net moment to zero. The angle θ_2 will maintain the cylinder in a circular path. A numerical technique is used to solve the above integral because an analytical solution was not found.

5.2.2 Sensorless Behaviors

The previous analysis will serve as a guide to design the sensorless behaviors for the 4-jointed hand.

Grasping Region

The proposed behavior takes advantage of the second finger joint.

θ_2, the angle between the first and second joint, is found solving equation (5.8) iteratively. The following algorithm is proposed to find θ_2:

1. Pick an initial angle θ_2 between 0° and 90°, because the solution will be between those two values.

2. Solve equation (5.8) numerically using the above guess for θ_2 .

3. If the solution to equation (5.8) is positive, decrease θ_2. A positive solution indicates that a positive moment is applied to the cylinder which will cause it to roll in (towards the palm of the hand). A negative solution will have the opposite effect.

4. Repeat the last to find the angle θ_2 that will set the net moment to zero.

The hand motion would consist of closing the first joint at a constant angular velocity. Upper limits on closing speeds will be determined experimentally in the following chapter.

The contact grasping region for this behavior is just a disk of radius:

$$R_c = \sqrt{L_1^2 + L_2^2 + 2L_1L_2\cos(\theta_2)}$$

It has been assumed that the fingers can actually rotate a full 180° and move on different planes. If the hand doesn't have such capabilities (ie finger joint limits), the pre-image would be reduced accordingly. An example is not provided for this behavior because of its simplicity; but the following chapter will provide experimental results for this pre-image.

5.2.3 Sensory

Again, all behaviors derived for the 2-jointed hand can be used for a 4-jointed hand. The following proposed behavior does not increase the size of the pre-image but it increases the robustness during the acquisition phase.

1. Open the hand to its full extent which would correspond to setting $\theta_2 = 0$.
2. Close θ_1 until one of the sensors triggers.
3. If the sensor on the first link or on the wrist triggers, close the second link until it makes contact with the cylinder; then close the first link.

4. If the sensor on the second link triggers, stop closing the first joint and close the second joint to angle θ_2 (found as outlined in the previous section); then close the first joint.

A 4-jointed hand with sensors has advantages over the sensorless version, unlike the 2-jointed hand. The second link of the finger is being used to increase the grasp's robustness. This same strategy should be superimposed for behaviors based on arm motion for a 4-jointed hand. This superposition of behaviors is somewhat analogous to Brooks's[86] subsumption architecture. The behaviors are triggered according to the hand's geometric complexity.

5.3 Zero-G Grasping

5.3.1 Sensorless

Three different grasp strategies are proposed. The first has an analytical basis and the other two depend on simulation results.

1. Close the second joint to an angle θ_{2a} that makes the tangential acceleration equal to zero. θ_{2a} is found to be:

$$\theta_{2a} = \arccos\left(-\frac{L_1}{L_2}\right)$$

Then close θ_1 the angle for the first finger joint. θ_{2a} was computed such that the centrifugal force due to the rotation of the first link, always points in a direction perpendicular to the second link.

For this type of behavior L_1 must also satisfy the following:

$$R\tan\left(\frac{\theta_2}{2}\right) \leq L_1 \leq L_2$$

2. The second strategy decouples the motion of each joint. Close the second finger to a specified angle which is somewhat arbitrary and has to be determined iteratively for a given hand geometry. Then close the first link. This a two part independent motion of the finger links.

3. This last strategy couples the motion of the two joints. Close the the first and second finger joints at a constant angular velocity ratio. Intuitively, ratios of $\frac{\dot{\theta_2}}{\dot{\theta_1}}$ greater than or equal to one should be used. Simulation of the dynamics is required to obtain the pre-image using this type of motion.

Given the dimensions of a hand, all three proposed behaviors should be evaluated in order to select the optimal (ie. largest) pre-image.

5.3.2 Sensory

On top of the already proposed strategies for the 2-jointed hand, the sensors on the second finger should again be used to increase the robustness of the acquisition phase.

The following behavior is designed for special initial conditions of the cylinder. If it is assumed that the puck will be coming from a certain direction, the hand could be preshaped to redirect the puck towards the palm. Figure 5.10 illustrates the previous example.

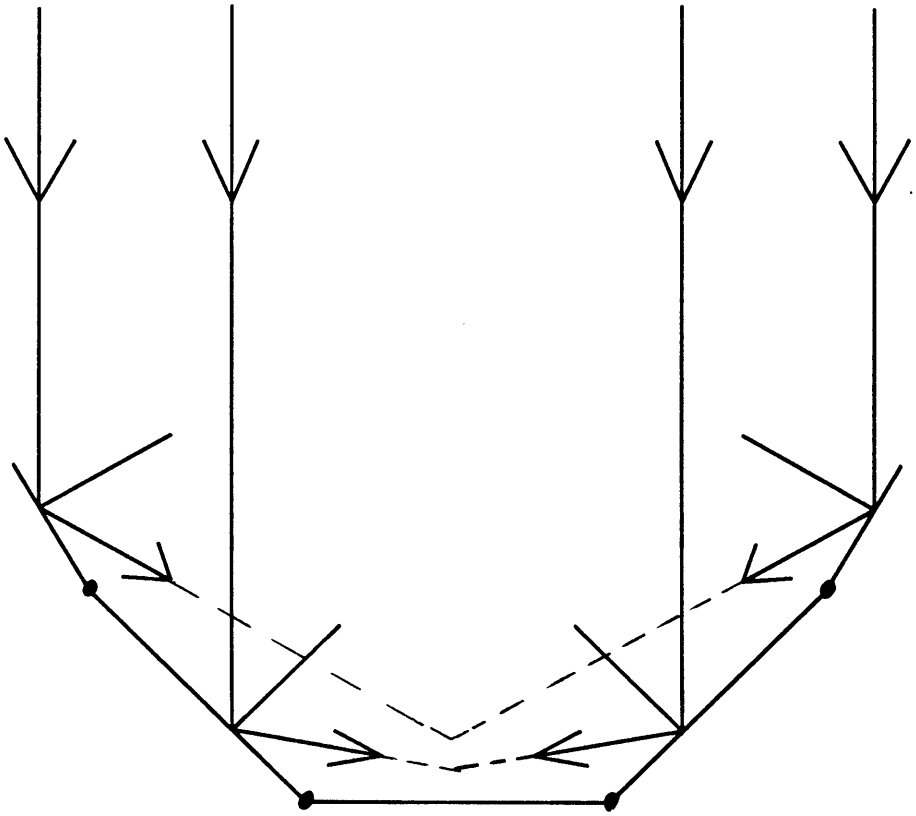

Figure 5.10: Behavior Conditioned for an Object Approaching Normal to the Wrist Surface

Chapter 6

2-D Implementation

This chapter tests the validity of the grasping regions using a 2-fingered hand. Pre-images for the 2-jointed and 4-jointed hand are investigated for quasi static and zero-G grasping behaviors. Bounds on the closing angular velocity of the joints will be determined experimentally.

6.1 Hardware Set-Up

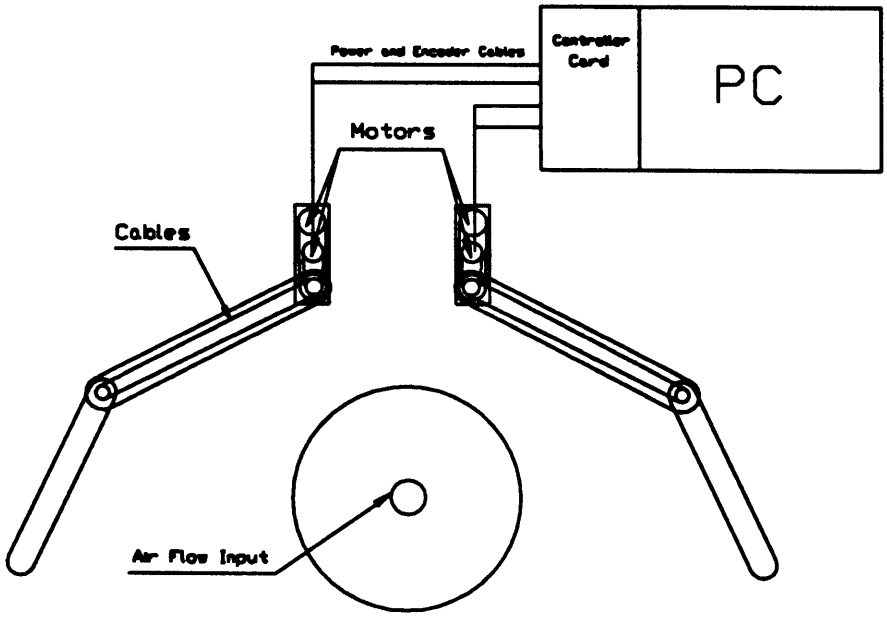

Figure 6.1: 2-D Experimental Set-Up

The experimental set-up is shown in figure 6.1. The 2-fingered (two joints per

finger) hand is the experimental equivalent of the 4-jointed hand model; but it can also serve as an experimental test bed for the 2-jointed hand. Unlike the theoretical model, the fingers do have a specified thickness. The wrist's dimension can be set arbitrarily, unlike the finger's dimensions. Hand/Arm behaviors cannot be tested with this set-up because the wrist is fixed to the table, but the next chapter will show an implementation of such behaviors. This chapter will focus on the sensorless behaviors.

Pulleys are used to transmit motor torque to the joints. The pulleys are the major reason for having thick fingers, but it should remembered that this is only a test bed. The effect of the finger thickness which was not included in the model, on the pre-images will be studied in later sections. The fingers move in the same plane which inhibits the acquisition of small objects. But for all practical purposes, any motion that geometrically encloses the object by the fingers will be considered successful.

A controller card employing HP,HCTL-1000 motor controller chip was used to implement the low level PID servo loops, and a front-end PC for the higher level commands. Each motor can be controlled independently. Collisions with the environment are detected by checking the commanded duty cycle of each motor. When the finger makes contact with the environment the motor current increases. Hence, final position, duration of motion, and a duty cycle need to be specified for each grasping motion.

A puck has been built to simulate zero-G in 2-D. A flexible air hose provides pressured air to support the weight of the puck. For small motions, the flexible hose has little effect on the puck's linear motion. It should be noted that the puck inhibits rotational motions greater than 90°. Since the puck moves at small velocities, air resistance is negligible. Aluminum weights have been added to the puck to increase the total momentum and to decrease the effects of air resistance and of the flexible

hose. The air pressure is turned off for quasi static grasping motions.

The following hand dimensions have been used throughout the experimental phase.

$$
\begin{aligned}
L_1 &= 13.7cm \\
L_2 &= 10.7cm \\
L_3 &= 6.0cm \\
R_b &= 3.8cm
\end{aligned}
$$

The same scale has been used on all the figures so that the size of the pre-images can be compared.

6.2 2-Jointed Hand

The pre-images developed earlier for the 2-jointed hand are now compared with the experimental results. The motion of the fingers has been coupled in order for the hand to behave like a 2-jointed hand.

The experimental results for the grasping regions were determined by trial and error. The following procedure was used:

1. The cylinder was placed on a marked location on the table.
2. The desired behavior was triggered.
3. If the motion ended in a successful grasp, the location was registered and a new trial was made with an initial location further away from the hand. If the motion was not successful, the location was deleted and a new trial was made with an initial location closer to the hand. This process was repeated until the limits of the grasping region were found.

6.2.1 Quasi Static Grasping

The behavior of closing the fingers at a fixed angular velocity is being studied. Figure 6.2 shows the difference between the predict and the experimental pre-image.

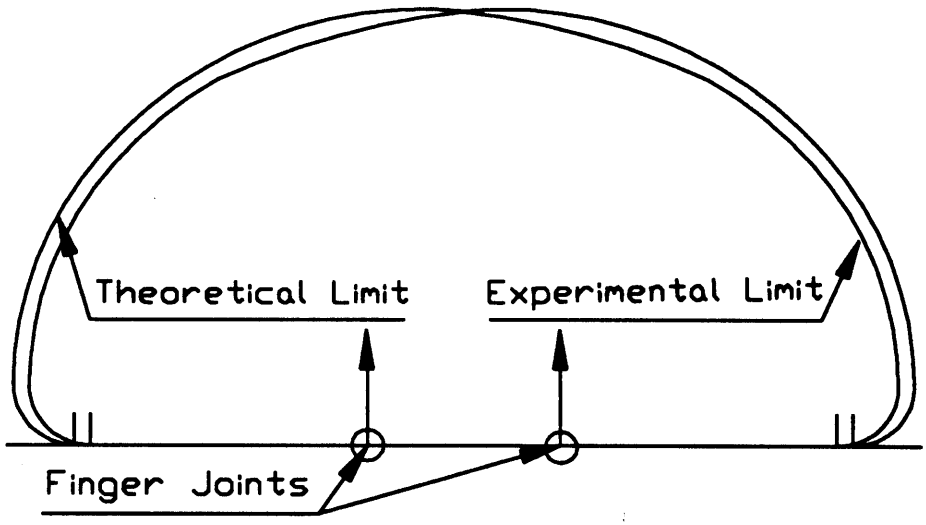

Figure 6.2: Experimental Quasi-Static Whole Grasping Region for a Sensorless 2-Jointed Hand

The experimental pre-image is at most one centimeter (radially) smaller than the theoretical result. This corresponds to a maximum error of about 5.5%. The error decreases for large angles of θ_1. The discrepancies are mainly due to:

1. Finger Thickness: The model assumed that the fingers are simple lines. This assumption alters the cylinder's motion from the theoretical prediction. The thickness is equal to 2.5 cm which is quite large relative to the finger size. Relatively smaller finger thickness would increase the predicted motion of the cylinder.

2. Friction: A uniform pressure distribution has been assumed during the analytical derivation. Uniform pressure distribution is hard to achieve which causes

deviations from the analytical solution.

As a result, the cylinder rotated by 15° instead of maintaining its orientation (as we had predicted). Closing rates up to 20°/second were used during the grasping motions. When higher closing rates were used the hand failed to acquire the cylinder because dynamic effects began to dominate.

The gap between the experimental and theoretical results can be bridged if a thinner finger link was used and if the sliding surface was made smoother.

6.2.2 Zero-G Grasping

Figure 6.3 shows the difference between the predicted and the experimental pre-image.

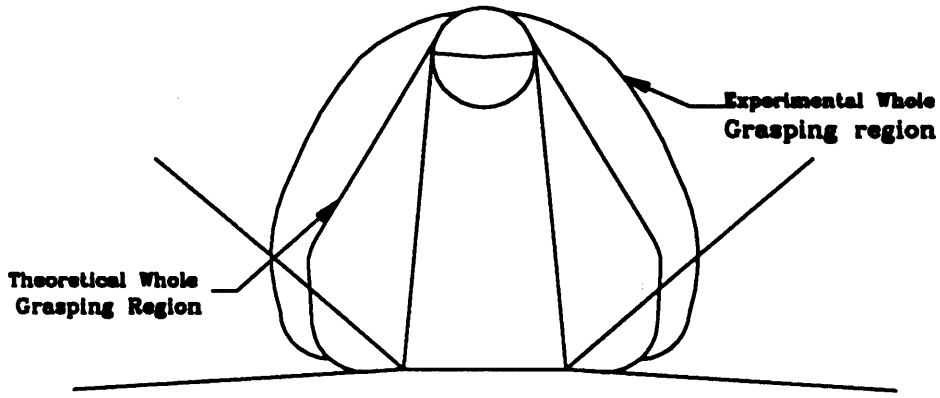

Figure 6.3: Experimental Zero-G Grasping Pre-Image for a Sensorless 2-Jointed Hand

The theoretical pre-image is somewhat conservative as expected. The theoretical pre-image is about 34% smaller (radially) than the experimental pre-image. These discrepancies are mainly due to:

1. Conservative assumptions in the model. The fingers were assumed infinitely massive during the impact and a coefficient of restitution of 1 was also assumed

. But, it was observed that the fingers would actually slow down. The fingers would absorb some of the impact energy which would imply that the puck would be imparted a slower exit velocity; and hence increase the size of the pre-image.

2. During impact, the puck would strike the surface before sliding away from the hand. This occurred because the impact created a moment that would tilt the puck on its side. This had the effect of slowing the puck which in turn gave the fingers ample time to catch up with it. This in turn increased the size of the pre-image.

The pre-image is therefore somewhere between the predicted and the experimental pre-image.

6.3 4-Jointed Hand

The first and second joints have been decoupled in order for the 2-Fingered hand to behave like the 4-jointed model.

The behavior that is now under investigation corresponds to the one derived in chapter 4. The behavior consists of curling the second joint to a prescribed angle θ_2 and then close the first joint at a fixed angular velocity. If the theory matches reality, the cylinder should move in a circular path.

The goal is to determine experimentally the angle θ_2 that pushes the cylinder in a circular path. This angle can be found by solving equation (5.8) for the angle θ_2 that reduces the double integral to zero (ie net moment on the cylinder equal to zero). An iterative solution as outlined is section 5.2.2 was used to solve for θ_2. *MACSYMA* was used to numerically integrate equation (5.8).

Using the hand dimensions, θ_2 was found to be 19.5°. θ_2 was determined experimentally to be 35°. The closing angular velocity was 1°/second.

This corresponds to an error of about 44.3%. This is somewhat unacceptable. I suspected that the finger thickness was the main cause for this discrepancy. When

the finger thickness is included in equation (5.8), θ_2 was found to be 28.5° which corresponds to an error of 18.6%. Hence, the correction for the finger thickness provides a much better approximation. This last discrepancy with the experimental value can be attributed to the non uniformity in pressure distribution and in some stiction properties.

This chapter presented sensorless grasping behaviors. Behaviors utilizing sensors will be discussed in the next chapter.

Chapter 7

Implementation on the Salisbury Hand

In this chapter, implementation issues on the *Salisbury Hand* (hardware/software) are discussed for the behaviors described in the previous chapters. A number of the sensory behaviors have been implemented and are discussed with respect to the 3-D implementation.

3-D grasping regions are built from an extension of the 2-D cases. Two types of grasping modes (tip prehension and cylindric) are used for this implementation. A cylindric grasp is a mode which occurs when the hand approaches a cylinder (assumed to be of infinite length) normal to its axis of rotation, while a tip prehension mode occurs when the hand approaches the cylinder (or a disk) from its end along its axis of rotation and uses three fingertips to constrain the disk.

These grasping modes combined with the sensory behaviors developed in earlier chapters were used in two examples. The tip prehension mode was used to grasp a cylinder lying on a table top, while the cylindric mode was implemented to grasp a "free floating" cylinder.

7.1 Experimental Set-Up

7.1.1 Hardware

A schematic of the experimental set-up is shown in Figure 7.1 and is mainly composed of three subsystems: the Salisbury hand, a Puma arm, and a vision system.

The Salisbury hand has three fingers with three degrees of freedom per finger. The Puma 560 arm has six degrees of freedom. The hand is mounted on the arm. A

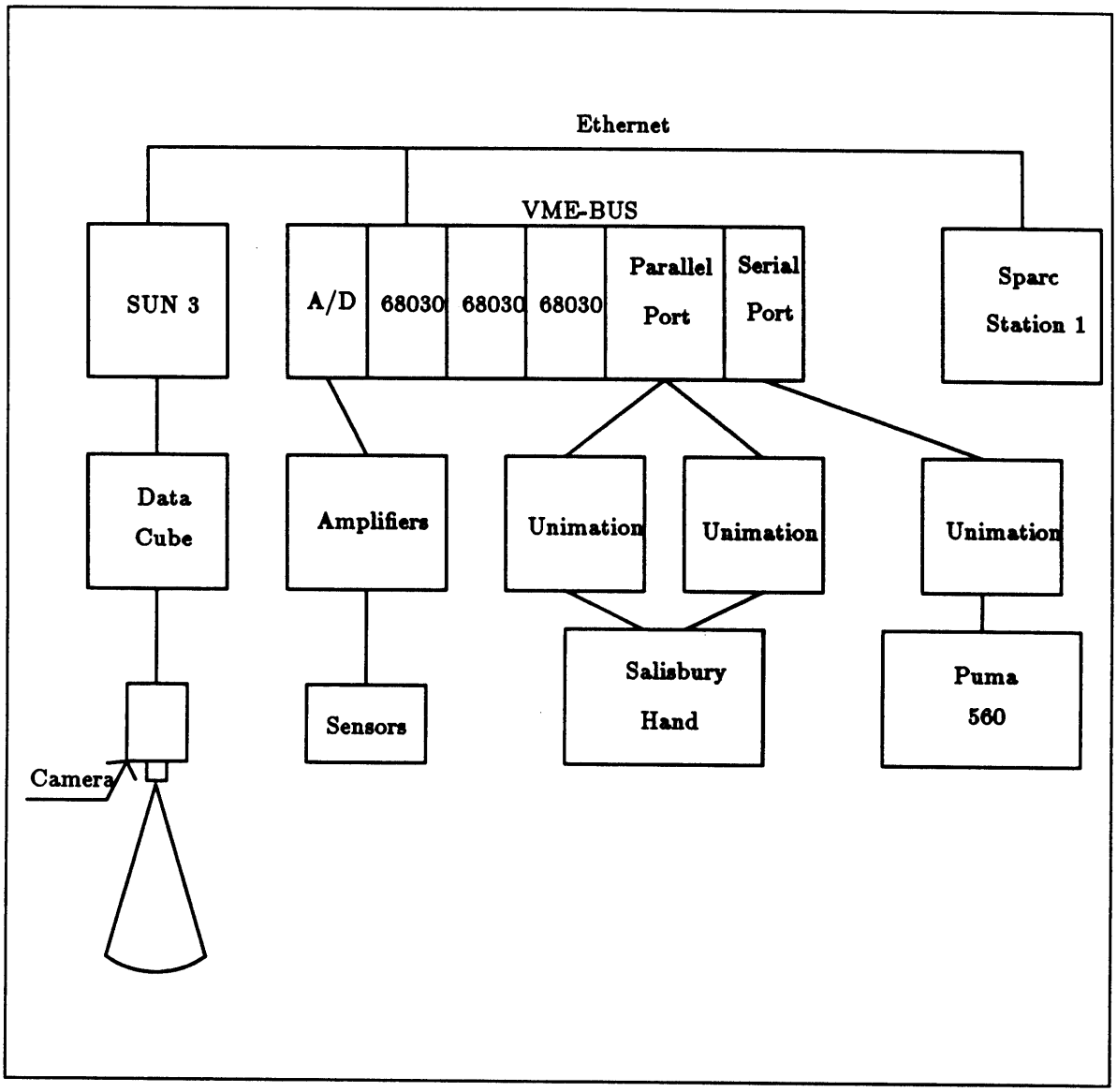

Figure 7.1: 3-D Experimental Set-Up

commercially available vision system (Datacube) was used to determine actual object locations to be input into the grasping system. Collisions with the environment are monitored using hand sensors including the tendon tension sensors, and a palm contact sensor.

A VME-bus-based multi-processor system (using three 68030 processors) with a Sun Workstation front-end in conjunction with three Unimation control boxes coordinate the mechanical components. The Unimation boxes handle the low level PID servo loops to control the hand and arm motors. The processors are connected to the Unimation controller via serial and parallel ports. The processors implement the higher level commands and enables tight coupling between sensory events and motor actions.

The vision system runs on a SUN-3 which interacts with the VME-bus via the Ethernet.

7.1.2 Software

Vx-Works, a real-time operating system, is used to control and coordinate the mechanical hardware components. Communication across the backplane can be achieved at a rate of 320 MBytes/sec.

The Puma arm is controlled using the Alter Mode protocol. In Alter Mode, the Unimation box sends a message to the processors every 28 ms requesting a position update. If a new position is not supplied within 15 ms from the Unimation's request, the communication gets interrupted. The maximum bandwidth of the system is therefore limited by the 28 ms. update rate of the controllers. The same type of limitations are also imposed on the hand. The overall performance of the system is limited by this connection.

The processors generate Remote Procedure Calls (RPC) via the Ethernet connection to feed the object's coordinates to the system. The frame rate for this system is

on the order of 30Hz, depending on the load from other users.

7.2 Extensions to 3-D Grasps

The extensions are at two levels. First, we extend the 2-D grasping regions to 3-D. Then, we discuss how to re-orient the hand wrist given sensory information. We have to note that these extensions apply to some simplified 3-D motions. The assumptions that we make are as follows:

1. The fingers are constrained to move in the same plane. In the case of the Salisbury hand, the motion of the fingers is coupled, such that the degrees-of-freedom are reduced to three, which are used to curl the fingers around the cylinder.

2. The cylinder is assumed to be of infinite length. Naturally, this doesn't have to be the case; and for practical purposes the cylinder's height should be at least twice as large as the width of the hand. This assumption is made to prevent the cylinder from slipping in between the fingers.

These assumptions limit the hand's full capabilities but they are sufficient for the implementation of primitive grasps. We now extended the 2-D grasping behaviors to 3-D.

The 3-D grasping regions are constructed using results derived in the 2-D analysis. The cylinder is sliced along a plane parallel to its base. Each slice can be viewed as a 2-D case. Therefore, the 2-D grasping regions are stacked along the plane of each slice. The 3-D grasping region is obtained by projecting the 2-D grasping region along the cylinder's major axis of symmetry. This assumes that the hand approaches the cylinder in the same plane as the cylinder's base. An example is provided in Figure 7.2, which is the 3-D extension of the 2-D case presented in Figure4.4.

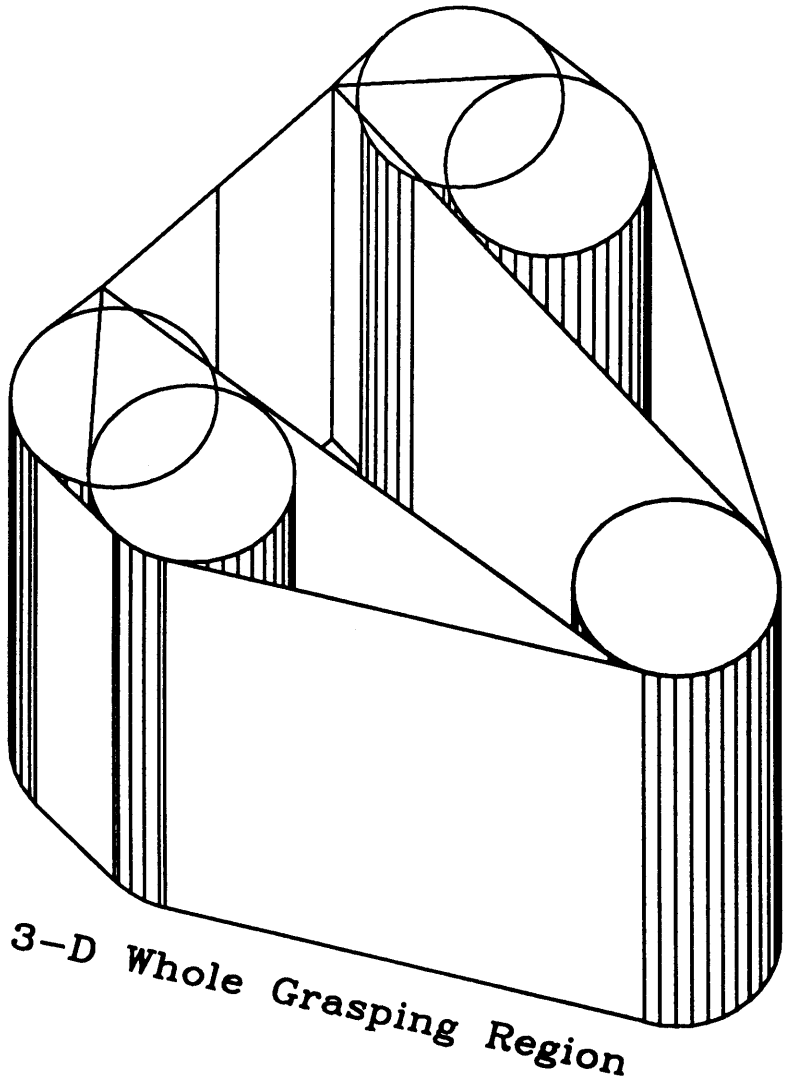

Figure 7.2: 3-D Zero-G Pre-Image for a Sensorless Hand

We also present a new behavior that will re-orient the hand in a plane parallel to the cylinder's base. This new orientation was assumed in the derivation of the 3-D grasping region. This behavior requires at least two touch sensors to be present on two opposite sides of the palm. The robot only recognizes that it has contacted the object when one or both of its palm-touch sensors has been activated. If *both* sensors

are activated, the robot assumes that it has reached the proper orientation before grasping the object in a stable manner. On the other hand, if only *one* of the sensors has been activated, then the robot needs to move its hand so that a stable grasp is obtained. To do this, it rotates the hand about the point of contact (i.e., at the sensor that has detected the contact) until the other sensor also comes in contact. This behavior will correct the hand's motion if it is approaching the cylinder in a plane not parallel to the cylinder's base.

7.3 Implementations

We present two sensory based behaviors on the Salisbury hand. The first one involves picking up a cylinder lying on a table, and the second one grasping a cylinder that is suspended from the ceiling (ie simulating a zero-G grasp).

7.3.1 Grasping a Cylinder on Constrained Surface

The analysis presented in previous chapters was used to derive pre-images for cylinders. In our implementation, the hand approaches the cylinder in a direction that is parallel to its axis of rotation. From such an approach the cylinder appears to be a disk. Hence we use the same style as the analysis presented in section 3.4.2.

The sensing is done using finger tendon tensions, and a palm sensor. The noise in the tension sensors reduces the sensitivity to finger contact. In fact, the finger exerts a relatively large force before sensing the cylinder. This causes the cylinder to slide or fall over during finger contact. These problems practically reduce the size of the pre-image.

Because we are not addressing the obstacle avoidance problem, objects will be placed in an obstacle-free environment. The object's coordinates are fed to the system using the vision system. The hand is oriented so that the three finger tips lie in a plane parallel to the constrained surface (a table in our case). Then the arm moves

towards the table until the hand touches the object. Depending on which sensor triggers appropriate action is taken. If the palm touches the cylinder, the fingers close. If two fingers touch, then one arm motion is required to grab the cylinder. In the event that only one finger touches, then another arm motion is required to reduce the uncertainty in the cylinder's position. A maximum of two approaches are needed to acquire the object given the present sensory capabilities.

The implementation was quite successful, but it failed at times because the cylinder would fall over when the fingers touched the rim.

7.3.2 Grasping a Free Floating Cylinder

To simulate zero-g grasping, a bar was hung from the ceiling on which a cylinder was tied on one side, with a counter weight on the other side. This mechanism gave the cylinder the ability to move somewhat like a "free-floating" object in the neighborhood of its equilibrium position.

The palm was the only sensor used in this implementation because it was sensitive enough to detect the collision with the cylinder before it bounced away. This reduces the pre-image size to the width of the palm.

The Puma arm was driven in the direction of the cylinder's equilibrium position. While the arm was moving, the palm sensor was continuously sampled to check for collisions with the object. When a force was detected, the fingers were commanded to close while the arm was moving. The arm's motion was ended when the fingers reached their final position. This implementation was also very successful. It failed at times when the arm was mis-aligned with respect to the cylinder's equilibrium position. It was also found that the success of this implementation was not very sensitive to the wrist orientation. This is mainly due to the experimental set-up, and in a real zero-g environment the wrist's orientation would affect the cylinder's motion.

Chapter 8

Conclusion

8.1 Review

In this thesis we have described and implemented reflexive grasping behaviors for planar 2-D grasping and then for simplified 3-D.

Chapter 2 established the necessary geometric and friction conditions for grasping cylinders with a 2-jointed hand and established the lower and upper bounds on the range of object sizes that can be acquired given a hand geometry; this concept was also extended to convex polygons.

Chapter 3 defined a region relative to the hand known as the grasping pre-image. If an object to be grasped is placed within this pre-image and the appropriate grasping behavior is initiated, successful object acquisition is guaranteed. The cylinder's motion was assumed to be friction dominated (quasi-static). We then defined and analyzed how sensorless and sensory based behaviors affect the shape and size of the grasping pre-image.

Chapter 4 developed sensorless and sensory behaviors for grasping cylinders in a zero-G-like environment (space).

Chapter 5 examined the same issues discussed in chapters 2, 3, and 4 but for a more complex 4-jointed hand.

In chapter 6, a planar 2-fingered hand was used to implement and test the concepts derived in earlier chapters.

Chapter 7 extended the 2-D analysis to 3-D cases which were successfully implemented on a robot system consisting of the Salisbury hand, a Puma 560, and a vision

system.

8.2 Future Work

While this work has clearly demonstrated the feasibility of automatic grasping, it suggests several areas of investigation which must be pursued to make this style of object acquisition truly practical:

1. **Hand Model.** Our current model of the hand employs two joints and assumes the links are simple lines. More accurate models would permit less conservative construction of pre-images. While the spirit of our approach is to employ the minimum level of complexity necessary to formulate successful behaviors, modeling of the inner joints and third finger would make available a broader class of reflexes.

2. **Behaviors.** The behaviors we have considered so far are simple one- or two-step hand closures. More subtle multi-step and continuous behaviors should be considered. We have looked at the problem of developing behaviors given a task and a hand structure. It would be interesting to look at problem like : " What is the minimum (least number of links) structure that would achieve a given task?", or "What kind of sensing is required to achieve a given task?".

3. **Grasp Stability.** While we have emphasized object acquisition, it is also important to consider active ways to improve the stability of a given grasp. It should be possible to improve a force closure grasp by proper fingertip force reallocation and in some cases it may be possible to draw an object held in a force closure grasp into a more secure form closure grasp. At a minimum we should also detect slipping and failed acquisition.

4. **Control Architecture.** A new control architecture is needed to ease the integration of these reflexive behaviors with some high level planner. A well

thought out hierarchy of sensory response and motor control processes should permit construction of reflexes more suitable for implementation. A new programming language is required to simplify the coordination of such complex robot systems.

5. **Hardwired Behaviors.** The behaviors could be hardwired directly into the system. The sensors could be directly linked to the actuators with dedicated electronics to determine the appropriate behavior. Behaviors could also be mechanically built-in the system; this would eliminate computation and processing time. Greiner[90] built a finger with mechanical built-in curling grasping behaviors. This is a very interesting idea, and work should be pursued in that direction to develop more versatile robot end-effectors.

6. **Arm Workspace.** Various constraints on arm motion, such as joint and workspace limits affect the feasible pre-image and should be included in the construction of the pre-image.

References

1. **Brock, D. L.** "Enhancing the Dexterity of a Robot hand Using Controlled Slip," *Technical Report 992*, MIT Artificial Intelligence Laboratory, Cambridge, MA, May, 1987.

2. **Brooks, R. A.** "Achieving Artificial Intelligence Through Building Robots," *A.I. Memo 899*, MIT Artificial Intelligence Laboratory, Cambridge, MA, May, 1986.

3. **Brost, R. C.,** "Automatic Grasp Planning in the Presence of Uncertainty," IEEE, 1986.

4. **Buhler, M., and Koditschek, D.E., and Kindelmann, P.J.** "Planning and Control of Robotic Juggling Tasks," In H. Miura, editor, *Fifth International Symposium on Robotics Research*, MIT Press, Tokyo, Japan, 1989.

5. **Buhler, M., and Koditschek, D.E., and Kindelmann, P.J.** "A Simple Juggling Robot: Theory and Experimentation," *The First International Symposium on Experimental Robotics*, Montreal, Canada, June 1989.

6. **Cutkosky, M. R., and Wright, P. K.** "Friction, Stability and the Design of Robotic Fingers," *The International Journal of Robotics Research*, Vol. 5, No. 4, Winter 1986.

7. **Dedieu, E., Degrange, P., Sailly, F.,**"Etude Sur Les systemes Comportementaux," Rapport du Project de Troisieme Annee ENSIMAG, France, 1989.

8. **Eppinger, S.D.,**"Modeling Robot Dynamic Performance for Endpoint Force Control," Technical Report 1072, MIT Artificial Intelligence Laboratory, Cambridge, MA, August 1988.

9. **Erdmann, M. A., and Mason, M.T.,**"An Exploration of Sensorless Manipulation," IEEE Journal of Robotics and Automation, Vol.4, No.4, August 1988.

10. **Fearing, R.S.,**"Simplified Grasping and Manipulation with Dextrous Robot Hands," *A.I. Memo 809* , MIT Artificial Intelligence Laboratory, Cambridge, MA, November, 1984.

11. **Fearing, R.S.,**"Implementing a force strategy for object re-orientation," In *Proc IEEE Intl. Conference on Robotics and Automation* , San Francisco, April 1986.

12. **Gordon, S.J.,**"Robotic Testbed for Adaptive Grasping of Objects in Space," Phase II Proposal by Intelligent Automation Systems, Inc., 1989.

13. **Greiner, H.,**"Passive and Active Grasping with a Prehensile Robot End-Effector," *M.S. Thesis*, MIT, Department of Electrical Engineering and Computer Science, Cambridge, MA, 1990.

14. **Johnson, R.C.,**"Impact Forces in Mechanisms," Machine Design, June 12, 1958.

15. **Kahng, J., and Amirouche, F.M.L.**"Impact Force Analysis in Mechanical Hand Design" In *IEEE*, 1987.

16. **Kerr, J., and Roth, B.** "Analysis of Multifingered Hands," The International Journal of Robotics Research, Vol. 4, No. 4, Winter 1986.

17. **Mason, M.T.,** "Manipulator grasping and pushing operations," Technical Report AI-TR-690, MIT Artificial Intelligence Laboratory, Cambridge, MA, June 1982.

18. **Lozano-Perez, T.,** "*Spatial Planning*: A configuration Space Approach," IEEE Transactions On Computers, Vol. C-32, No. 2, pp. 108-120, February, 1983.

19. **Lozano-Perez, T., Mason M.T., and Taylor, R.H.** "Automatic Synthesis of Fine-Motion Strategies for Robots," The International Journal of Robotics Research, Vol. 3, No. 1, pp. 3-24, Spring, 1984.

20. **Mason, M.T., and Salisbury, J.K.,** "Robot Hands and the Mechanics of Manipulation," , MIT Press, Cambridge, MA, 1985.

21. **Narasimhan, S.,** "Dexterous Robotic Hands: Kinematics and Control," *Technical Report 1056*, MIT Artificial Intelligence Laboratory, Cambridge, MA, 1988.

22. **Parker, J.K., and Paul, F.W.,** "Impact Force Control in Robot Hand Design," ASME Conference, Robotics and Manufacturing Automation, vol. 15, Nov. 1985, pp. 57-65.

23. **Peshkin, M.A., and Sanderson, A.C.,** "Planning Robotic Manipulation Strategies for Workpieces that Slide," IEEE Journal of Robotics and Automation, VOL. 4, No. 5, October, 1988.

24. **Peshkin, M.A., and Sanderson, A.C.,** "The Motion of a Pushed, Sliding Workpiece," IEEE Journal of Robotics and Automation, VOL. 4, No. 6, December, 1988.

25. **Pollard, N.S.,** "Maneuvering and Grasping: Toward Task-Level Programming for an Articulated Hand," *S.M. Thesis,*, Dept. of Electrical Engineering and Computer Science, MIT, Cambridge, MA, August 1988.

26. **Siegel, D. M.** "Finding the Pose of an Object in a Hand," *Phd. Proposal*, MIT Artificial Intelligence Laboratory, Cambridge, MA, 1990.

27. **Stansfield, S. A.** "Robotic Grasping of Unknown Objects: A Knowledge-Based Approach," *Sandia Report SAND89-1087*, Albuquerque, NM, June 1989.

28. **Sundaram, K.** "The Use of Joint Torque Feedback for Force Control," *M.S. Thesis*, MIT, Mechanical Engineering Dept., Cambridge, MA, May, 1990.

29. **Trinkle, J.C.** "A The Object Motion Problem: A New Formulation for the Analysis Quasi-Static Systems of Rigid Bodies in Contact," Department of Systems and Industrial Engineering, University of Arizona Tucson, AZ, Working Paper 89-020, August 1989.

30. **Van-Duc Nguyen,** "The synthesis of stable force-closure grasps," *Technical Report AI-TR-905*, MIT Artificial Intelligence Laboratory, Cambridge, MA, July 1986.

31. **Wang, Y.** "Dynamic Analysis and Simulation of Mechanical Systems with Intermittent Constraints," *Phd. Dissertation*, Dept. of Mechanical Engineering, The Robotics Institute, Carnegie Mellon University, May 1989.